The corresponding 9,13-dicis aldehyde **16a** was also reacted with *n*-butylamine according to method A. The initial ^{1}H NMR spectrum in C_6D_6 revealed the presence of the same 9-*cis*-DHP-**15b** (>80%) admixed with <20% of what is presumably 9,13-dicis Schiff base **16b** (H_{15} doublet, $J \sim 9$ Hz, at δ 8.4). After 30 min at room temperature, only a trace of **16b** remained, and the latter was completely absent after 90 min wherein the ^{1}H NMR spectrum of the resulting 9-*cis*-DHP-**15b** was identical with that produced from 9,11,13-*tricis*-**14b**.

Dihydropyridinium Salt 19 by Protonation of DHP-7b in CD_2Cl_2. DHP-**7b** was prepared in the usual way from **3a** and *n*-butylamine according to method A. The vacuum-dried DHP-**7b** was dissolved in CD_2Cl_2, and its ^{1}H NMR spectrum was recorded (300 MHz; residual protonated CD_2Cl_2 as internal standard at δ 5.33): δ 1.010 (9 H, *t*-Bu, s), 1.007 (6 H, 2C_1-Me, s), 1.70 (3 H, 3 H_{18}, s), 1.81 (3 H, 3 H_{19}, d, $J \sim 1.1$ Hz), 2.77 (1 H, first diastereotopic hydrogen α to nitrogen of *n*-Bu, ddd, $J \sim 13.9$, 8.0, and 6.4 Hz), 2.95 (1 H, second diastereotopic hydrogen α to nitrogen of *n*-Bu, ddd, $J \sim 13.9$, 8.0, and 6.4 Hz), 4.61 (1 H, H_{14}, dd, $J \sim 7.5$ and 2.1 Hz), 4.66 (1 H, H_{12}, dd, $J \sim 5.0$ and 2.1 Hz), 4.81 (1 H, H_{11}, dd, $J \sim 9.4$ and 5.0 Hz), 5.75 (1 H, H_{10}, d, $J \sim 9.4$ Hz), 5.96 (1 H, H_{15}, d, $J \sim 7.5$ Hz), 5.98 (1 H, H_8, d, $J \sim 16.2$ Hz), 6.10 (1 H, H_7, d, $J \sim 16.2$ Hz). This spectrum is similar to that recorded in $CDCl_3$ and C_6D_6 (Table III). The solution of **7b** in CD_2Cl_2 was treated with excess trifluoroacetic acid at ambient temperature, and then the ^{1}H NMR spectrum was again recorded, indicating the formation of what has been identified as dihydropyridinium salt **19**: δ 1.00 and 0.99 (6 H, C_1-Me_2, two s), 1.17 (9 H, *t*-Bu, s), 1.66 (3 H, 3 H_{18}, s), 1.97 (3 H, 3 H_{19}, d, $J \sim 1.0$ Hz), 2.60 (1 H, first diastereotopic H_{12}, dd, $J \sim 18.7$ and 4.2 Hz), 3.00 (1 H, second diastereotopic H_{12}, dd, $J \sim 18.7$ and 4.8 Hz), 3.7 (2 H, CH_2 α to nitrogen, m), 4.80 (1 H, H_{11}, ddd, $J \sim 9.9$, 4.8, and 4.2 Hz), 5.42 (1 H, H_{10}, d, $J \sim 9.9$ Hz), 5.98 (1 H, d, $J \sim 16.1$ Hz), 6.4 (2 H, H_7 and H_{14}, m), 8.4 (1 H, H_{15}, br m).

Acknowledgment. This study was supported by NIH Grant DK-16595. We acknowledge NATO for a postdoctoral fellowship to A.R.d.L. The Hoffmann-La Roche Co., Nutley, NJ, and Badische-Anilin und Soda Fabrik, Luwigshafen, West Germany, are also acknowledged for providing starting materials utilized in this study.

Registry No. **1a**, 116-31-4; **1b**, 61769-47-9; **1c**, 92216-32-5; **2a**, 472-86-6; **2b**, 68737-92-8; **2c**, 92098-20-9; **3a**, 106190-63-0; **3b**, 115018-97-8; **3c**, 115019-02-8; **4a**, 90736-88-2; **4b**, 115018-99-0; **4c**, 115019-04-0; **5a**, 113775-89-6; **5b**, 115075-01-9; **5c**, 115075-02-0; **6a**, 85236-10-8; **6b**, 115019-01-7; **6c**, 120120-49-2; (±)-**7b**, 115018-98-9; (±)-**7c**, 115019-03-9; (±)-**9b**, 115031-66-8; (±)-**9c**, 120120-50-5; (±)-**10b**, 115019-00-6; (±)-**10c**, 120120-51-6; **11a**, 514-85-2; **11b**, 68737-94-0; **11c**, 114127-33-2; **12a**, 564-87-4; **12b**, 68737-93-9; **12c**, 114128-95-9; **13a**, 23790-80-9; **13b**, 120201-10-7; **13c**, 120201-11-8; **14a**, 85236-12-0; **14b**, 120120-46-9; (±)-**15b**, 120120-47-0; **16a**, 90745-29-2; **16b**, 120120-48-1; **17**·$CF_3CO_2^-$, 120120-42-5; **18**·$CF_3CO_2^-$, 120120-43-6; **19**·$CF_3CO_2^-$, 120120-45-8.

A Spectroscopic, Photocalorimetric, and Theoretical Investigation of the Quantum Efficiency of the Primary Event in Bacteriorhodopsin

Robert R. Birge,* Thomas M. Cooper, Albert F. Lawrence, Mark B. Masthay, Christ Vasilakis, Chian-Fan Zhang, and Raphael Zidovetzki

Contribution from the Department of Chemistry and Center for Molecular Electronics, Syracuse University, Syracuse, New York 13244. *Received July 15, 1988*

Abstract: The spectroscopic, photochemical, and energetic properties of the primary event of light-adapted bacteriorhodopsin (bR) are investigated with pulsed laser cryogenic photocalorimetry, photostationary-state spectral analysis, INDO–PSDCI molecular orbital theory, and semiempirical molecular dynamics theory. The principal goal is to explore the photophysical origins of the controversy concerning the primary quantum yield. The ratio of the forward to reverse quantum yields (Φ_1/Φ_2) of bR is observed to equal 0.45 ± 0.03 at 77 K in glycerol/water solution. Thus, Φ_1 must be less than 0.48 under these experimental conditions. The mole fraction of K (χ_K^{500}) in the 77 K, 500-nm photostationary state is observed to equal 0.46 ± 0.04. The calculated absorption spectrum of K at 77 K has a maximum absorbance at 620 nm and a molar absorptivity at λ_{max} of 63 900 M^{-1} cm^{-1}. The oscillator strength associated with excitation into the λ_{max} band f_K is determined to be 0.95 on the basis of log-normal regression analysis. The corresponding values for bR at 77 K are λ_{max} = 577 nm, ϵ_{max} = 66 100 M^{-1} cm^{-1}, and f_{bR} = 0.87. The observation that $f_K > f_{bR}$ is consistent with the displacement of the C_{15}=NH portion of the retinyl chromophore away from a negatively charged counterion as a consequence of the all-trans to 13-cis photoisomerization. It is difficult to reconcile the observation that $f_K > f_{bR}$ with the proposal that the primary event involves an all-trans to 13-cis,14-s-cis photoisomerization, because the latter geometry is predicted to have a significantly lower λ_{max} band oscillator strength relative to that of the all-trans precursor. Experimental and theoretical evidence is presented which suggests that two distinct forms of light-adapted bacteriorhodopsin may exist. We propose that these two forms have characteristic photocycles with significantly different primary quantum yields. INDO–PSDCI molecular orbital procedures and semiempirical molecular dynamics simulations predict that one ground-state geometry of bR undergoes photochemistry with a quantum yield Φ_1 of ~0.27 and that a second ground-state geometry, with a slightly displaced counterion, yields $\Phi_1 \sim 0.74$. This theoretical model may explain the observation that literature measurements of Φ_1 tend to fall into one of two categories—those that observe $\Phi_1 \sim 0.33$ or below and those that observe $\Phi_1 \sim 0.6$ or above. The observation that all photostationary-state measurements of the primary quantum yield give values near 0.3 and all direct measurements of the quantum yield result in values near 0.6 suggests that photochemical back-reactions may select the bacteriorhodopsin conformation with the lower quantum yield. We conclude that the primary photoproduct K has an enthalpy 15.9 ± 3.2 kcal mol^{-1} larger than that of bR at 77 K in agreement with our previous assignment (Birge, R. R.; Cooper, T. M. *Biophys. J.* **1983**, *42*, 61–69). However, we anticipate that this energy storage measurement is not necessarily valid for those environments yielding much higher quantum yields (e.g., $\Phi \geq 0.6$), and we suggest that energy storage in the latter situation is not only smaller but is likely to be insufficient to pump two protons under nominal in vivo conditions. The two photocycles may have developed as a natural biological requirement that *Halobacterium halobium* have the capacity to adjust the efficiency of the photocycle in relation to the intensity of light and/or membrane electrochemical gradient.

Bacteriorhodopsin is the light-harvesting protein of the purple membrane of the halophilic microorganism *Halobacterium halobium*.[1-5] The light-adapted form of this protein undergoes a complex photocycle (Figure 1) which transports one (or more) proton(s) across the membrane.[6] The primary structure of this protein is known,[7,8] and this information, along with spectroscopic

0002-7863/89/1511-4063$01.50/0

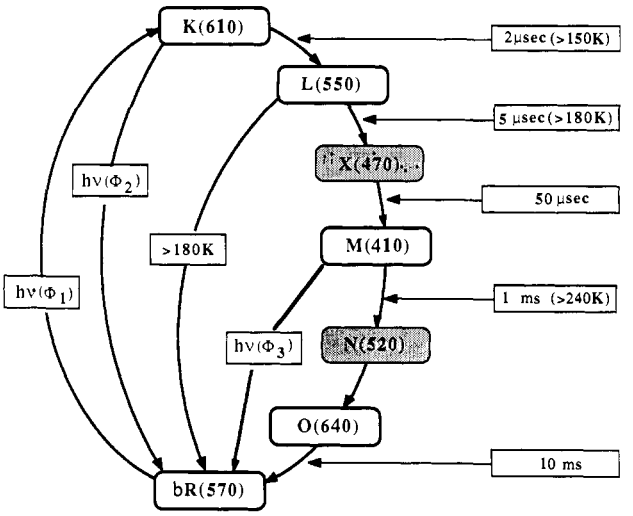

Figure 1. Photocycle of light-adapted bacteriorhodopsin. Individual species are indicated within the rectangular polygons, and the numbers in parentheses following the labels indicate the approximate absorption maxima in nanometers extrapolated to ambient-temperature environment. Species within shaded polygons are tentative, and relative free energies are related approximately to vertical position. Temperatures required for observing the formation of subsequent intermediates and the formation times extrapolated to ambient temperature are indicated for selected reactions. These temperatures and reaction times are approximate. Note that there is a major branching pathway that connects L directly back to bR and that under some experimental conditions this pathway dominates.

and theoretical studies of the molecular changes accompanying formation of the photocycle intermediates, provides for the possibility that the molecular mechanism of the proton pump can be elucidated.[2-5] This important goal, however, will be difficult to achieve in the absence of an accurate assignment of the quantum efficiency of the photoreaction, the proton translocation quantum yield, and the energetics of the primary event. All three variables are experimentally coupled such that accurate knowledge of the former is required in order to assign the latter two experimentally.[6,9]

Despite extensive experimental study,[10-19] assignment of the primary photochemical quantum yield (Φ_1 in Figure 1) of light-adapted bacteriorhodopsin remains a subject of controversy. As can be seen by reference to Table I, measurements of Φ_1 range from a low of 0.25[11] to a high of 0.79.[16] This measurement range is in sharp contrast to the agreement that is observed in the literature with respect to the measurement of the primary quantum yield for vertebrate rhodopsin photochemistry.[2,3,13,20] A closer examination of the data presented in Table I indicates that all of the direct experimental measurements fall into one of two categories—those that predict $\Phi_1 = 0.33$ or below and those that predict $\Phi_1 = 0.6$ or above. No experimental measurements fall into the large intermediate range spanning from 0.34 to 0.59. If experimental uncertainty were the dominant source of the discrepancies in the measured quantum yields, one would predict that a majority of the measurements would fall into this intermediate range in contrast to none at all.

In this paper, we use a combination of pulsed laser cryogenic photocalorimetry and photostationary-state (PSS) spectral analysis to assign three photophysical variables associated with the primary event of bR: Φ_1/Φ_2, $\Delta H_{12}(\Phi_1)$, and χ_K^{500}. We also present molecular dynamics simulations of the primary event which provide a possible explanation for why experimental measurements tend to yield $\Phi_1 \sim 0.3$ or $\Phi_1 \sim 0.7$, while excluding intermediate values. In addition, we determine the absorption spectrum of K (77 K) and demonstrate that this photoproduct has a λ_{max} band oscillator strength greater than that observed for bR (77 K). While this observation may appear to represent an anomaly given the all-trans to 13-cis photoisomerization that accompanies the primary event, molecular orbital calculations indicate that this increase in oscillator strength is consistent with the displacement of the C_{15}=NH portion of the retinyl chromophore away from a negatively charged counterion. Finally, we reexamine the issue of energy storage in the primary event. This reexamination is necessary because the energy storage value determined via photocalorimetry is sensitive to both Φ_1 and Φ_1/Φ_2. We conclude that our original measurement[9] of $\Delta H_{12} \sim 16$ kcal mol^{-1} is valid for those environments that select photocycles with primary quantum yields near 0.3. We suggest that this energy storage measurement is not necessarily valid for those environments yielding much higher quantum yields and predict further that energy storage in the latter cases in not only smaller but is likely to be insufficient to pump two protons under nominal in vivo conditions.

Experimental Section

Bacteriorhodopsin was isolated from the R1 strain of *Halobacterium halobium* following the procedures of Becher and Cassim.[21] All spectroscopic measurements were carried out at 77 K with protein dissolved in 2:1 glycerol/water (v/v).

Photostationary-state measurements were carried out at 77 K with an optical dewar filled with liquid nitrogen. At liquid nitrogen temperatures,

(1) For reviews, see ref 2. For recent studies of the binding site and the primary photochemical event in light-adapted bacteriorhodopsin, see ref 3-5.

(2) (a) Ottolenghi, M. *Adv. Photochem.* **1980**, *12*, 97-200. (b) Birge, R. R. *Annu. Rev. Biophys. Bioeng.* **1981**, *10*, 97-200. (c) Stoeckenius, W.; Bogomolni, R. *Annu. Rev. Biochem.* **1982**, *52*, 587-616. (d) Lanyi, J. K. In *New Comprehensive Biochemistry*; Ernster, L., Ed.; Elsevier: North-Holland, Amsterdam, 1984; pp 315-350.

(3) (a) Smith, S. O.; Braiman, M. S.; Myers, A. B.; Pardoen, J. A.; Courtin, J. M. L.; Winkel, C.; Lugtenburg, J.; Mathies, R. A. *J. Am. Chem. Soc.* **1987**, *109*, 3108-3125. (b) Baasov, T.; Sheves, M. *J. Am. Chem. Soc.* **1987**, *109*, 1594-1596. (c) Dewey, T. G. *Biophys. J.* **1987**, *51*, 809-815. (d) Baasov, T.; Sheves, M. *Biochemistry* **1986**, *25*, 5249-5258. (e) Albeck, A.; Friedman, N.; Sheves, M.; Ottolenghi, M. *J. Am. Chem. Soc.* **1986**, *108*, 4614-4618. (f) Liu, R. S. H.; Earnest, T. N.; Roepe, P.; Braiman, M. S.; Gillespie, J.; Rothschild, K. J. *Biochemistry* **1986**, *25*, 7793-7798. (g) Mead, D.; Asato, A. E. *J. Am. Chem. Soc.* **1985**, *107*, 6609.

(4) (a) Kouyama, T.; Nasuda-Kouyama, A.; Ikegami, A.; Methew, M. K.; Stoeckenius, W. *Biochemistry* **1988**, *27*, 5855-5863. (b) Fodor, S. P. A.; Pollard, W. T.; Gebhard, R.; van den Berg, E. M. M.; Lugtenburg, J.; Mathies, R. A. *Proc. Natl. Acad. Sci. U.S.A.* **1988**, *85*, 2156-2160. (c) van der Steen, R.; Biesheuvel, P. L.; Mathies, R. A.; Lugtenburg, J. *J. Am. Chem. Soc.* **1986**, *108*, 6410-6412. (d) Harbison, G. S.; Smith, S. O.; Pardoen, J. A.; Courint, J. M. L.; Lugtenburg, J.; Herzfeld, J.; Mathies, R. A.; Griffin, R. G. *Biochemistry* **1985**, *24*, 6955-6962.

(5) (a) Schulten, K.; Tavan, P. *Nature (London)* **1978**, *272*, 85-86. (b) Engelhard, M.; Gerwert, K.; Hess, B.; Kreitz, W.; Siebert, F. *Biochemistry* **1985**, *24*, 400-407. (c) Tavan, P.; Schulten, K. *Biophys. J.* **1986**, *50*, 81-89.

(6) Marinetti, T. *Biophys. J.* **1987**, *51*, 875-881; *52*, 115-121. Marinetti, T.; Mauzerall, D. *Proc. Natl. Acad. Sci. U.S.A.* **1983**, *80*, 178-180. Bogomolni, R. A.; Baker, R. A.; Lozier, R. H.; Stoeckenius, W. *Biochemistry* **1980**, *19*, 2152-2159. Govindjee, R.; Ebrey, T. G.; Crofts, A. R. *Biophys. J.* **1980**, *30*, 231-242.

(7) Ovchinnikov, Y. A.; Abdulaev, N. G.; Feigina, M. Y.; Kiselev, A. V.; Lobanov, N. A. *FEBS Lett.* **1979**, *100*, 219-224.

(8) Khorana, H. G.; Gerber, G. E.; Herlihy, W. C.; Gray, C. P.; Anderegg, R. J.; Nihei, K.; Biemann, K. *Proc. Natl. Acad. Sci. U.S.A.* **1979**, *76*, 5046-5050.

(9) Birge, R. R.; Cooper, T. M. *Biophys. J.* **1983**, *42*, 61-69.

(10) Hurley, J. B.; Ebrey, T. G. *Biophys. J.* **1978**, *22*, 49-66.

(11) Goldschmidt, C. R.; Kalisky, O.; Rosenfeld; Ottolenghi, M. *Biophys. J.* **1977**, *17*, 179-183.

(12) Goldschmidt, C. R.; Ottolenghi, M.; Korenstein, R. *Biophys. J.* **1976**, *16*, 839-843.

(13) Becher, B.; Ebrey, T. G. *Biophys. J.* **1977**, *17*, 185-191.

(14) Oesterhelt, D.; Hegemann, P.; Tittor, J. *EMBO J.* **1985**, *4*, 2351-2356.

(15) Polland, H.-J.; Franz, M. A.; Zinth, W.; Kaiser, W.; Kölling, E.; Oesterhelt, D. *Biophys. J.* **1986**, *49*, 651-662.

(16) Oesterhelt, D.; Hess, B. *Eur. J. Biochem.* **1973**, *37*, 316-326.

(17) Lozier, R. H.; Niederberger, W. *Fed. Proc., Fed. Am. Soc. Exp. Biol.* **1977**, *36*, 1805-1809.

(18) Iwasa, T.; Tokunaga, F.; Yozhizawa, T. *Biophys. Struct. Mech.* **1980**, *6*, 253-270.

(19) Dioumaev, A. K.; Savransky, V. V.; Tkachenko, N. V.; Chukharev, V. I. *Photochem. Photobiol.*, in press.

(20) Dartnall, H. J. A. In *Handbook of Sensory Physiology*; Dartnall, H. J. A., Ed.; Springer-Verlag: Heidelberg, 1972; Vol. VII, pp 122-145. Suzuki, T.; Callender, R. H. *Biophys. J.* **1981**, *34*, 261-265. Birge, R. R.; Callender, R. H. In *Biophysical Studies of Retinal Pigments*; Ebrey, T.; Frauenfelder, H.; Honig, B.; Nakanishi, K., Eds.; University of Illinois Press: Champaign, IL, 1987; pp 270-281.

(21) Becher, B.; Cassim, J. Y. *Prep. Biochem.* **1975**, *5*, 161-178.

Table I. Literature Assignments of Selected Photophysical and Spectroscopic Properties of Light-Adapted Bacteriorhodopsin

investigators[a]	Φ_1[b]	Φ_2[c]	Φ_1/Φ_2	T (K)[d]	reaction[d]	conditions[e]	λ_{max}(bR) (nm)	λ_{max}(K) (nm)	λ_{isos} (nm)[f]	χ_K
O&H (1973)	0.79		(>0.78)	300	bR → M	HS/ether	568			
GOK (1976)			0.40	300	bR ⇔ K	aqueous	568	590	592	
L&N (1977)				77	bR ⇔ K	aqueous	573	610	590	~0.5
B&E (1977)	0.30	0.77	0.39	233	bR ⇔ M	glycerol	568			
GKRO (1977)	0.25	0.63	0.40	300	bR ⇔ K	aqueous	570	590		
H&E (1978)	0.33	0.67	0.49	77	bR ⇔ K	glycerol	580	628	594	0.28
ITY (1980)				83	bR ⇔ K	glycerol	583	626	592	0.34
OHT (1985)	>0.6		(>0.6)	300	bR → M	HS/ether				
P et al. (1986)	~0.6		(>0.6)	300	bR → K	aqueous				
DSTC (1988)	0.31	0.93	0.33	296	bR ⇔ K	aqueous	568	580	590	
this work	<0.49		0.45	77	bR ⇔ K	glycerol	577	620	592	0.46

[a] Investigators are defined as follows: O&H (1973) = Oesterhelt and Hess (ref 16), GOK (1976) = Goldschmidt et al. (ref 12), L&N (1977) = Lozier and Niederberger (ref 17), B&E (1977) = Becher and Ebrey (ref 13), GKRO (1977) = Goldschmidt et al. (ref 11), H&E (1978) = Hurley and Ebrey (ref 10), ITY (1980) = Iwasa et al. (ref 18), OHT (1985) = Oesterhelt et al. (ref 14), P et al. (1986) = Polland et al. (ref 15), and DSTC (1988) = Dioumaev et al. (ref 19). [b] Quantum yield for the formation of the primary photoproduct, K, from bR. Some investigators assigned this value by measuring the quantum yield of the bR → M photoreaction and by assuming that the quantum yield for the bR → M photoreaction is identical with that for the bR → K reaction (i.e., no branching back to bR occurs during the dark steps). The individual references should be consulted for error range assignments. [c] Quantum yield for the formation of bR from the primary photoproduct, K. Some investigators assigned this value by measuring the quantum yield of the M → bR photoreaction and by assuming that the quantum yield for the M → bR photoreaction is identical with that for the K → bR reaction. The individual references should be consulted for error range assignments. [d] The measurement temperature and the photoreaction studied. The symbol ⇔ is used to represent a photostationary state. [e] Solvent conditions used in the experimental measurement. When specific solvent conditions are not provided, aqueous is assumed. HS represents high salt, and glycerol conditions are typically mixtures of glycerol and water. Individual references should be consulted for more detailed descriptions of the experimental conditions. [f] Isosbestic point observed for the absorption spectra of bR and the bR ⇔ K photostationary state.

the photocycle of light-adapted bacteriorhodopsin (Figure 1) is truncated at the primary photoproduct, and bR and K participate in the following photoequilibrium:

$$bR \underset{\Phi_2}{\overset{\Phi_1}{\rightleftharpoons}} K(\Delta H_{12}) \qquad (1)$$

where the symbol bR will be used throughout this paper to represent the light-adapted form of bacteriorhodopsin (i.e., $bR \equiv bR_{570} \equiv bR_{LA}$), K represents the primary photoproduct (i.e., $K \equiv K_{610}$), Φ_1 and Φ_2 are quantum yields of photoconversion, and ΔH_{12} represents the enthalpy stored in the primary photoproduct. Prior to spectroscopic analysis, the bacteriorhodopsin solution was irradiated for 20 min with broad-band excitation from a slide projector (Kodak 4400 projector) with a green gelatin filter slide inserted. Spectroscopic measurements of λ_{max} versus irradiation time indicate that 10-min irradiation times are sufficient to light adapt the protein fully. The protein/glycerol/water sample was cooled rapidly by injection into a precooled 3-mm path-length "lollipop" cell immersed in liquid nitrogen inside the dewar. After visual inspection to verify that the sample was optically clear and did not contain cracks, the dewar assembly was placed in the sample compartment of a computer-controlled McPherson EU-700 double-beam spectrophotometer. The $bR(bR_{LA})$ spectrum was then measured in 0.02-nm intervals with a spectral bandwidth of 0.2 nm and the final spectrum generated by averaging 10 scans from 350 to 780 nm. The monochromator was then replaced with the single-filter assembly. The 500-nm photostationary state was then generated by moving the lamp housing with filter assembly into optical contact with the double-beam module and directly irradiating the sample. Three different filter combinations were investigated: (filter 1) single 500-nm interference filter with a 12-nm FWHM band-pass (Ditric Optics, Inc., Hudson, MA), (filter 2) single 520-nm interference filter with a 10-nm FWHM band-pass (Ditric Optics), and (filter 3) a combination of filter 1 in series with a broad band-pass chemical filter (3 g of $K_2Cr_2O_2$ in 100 mL of H_2O; 10-cm path length; band-pass 350–580 nm). The latter was used to remove the very small amounts of blue radiation ($\lambda < 260$ nm) that are passed by the interference filter. The preparation of the photostationary state was monitored and the reaction continued for a time period twice that necessary to generate a constant absorbance reading. The filter assembly was then replaced with the monochromator in order to measure the photostationary-state spectrum in the wavelength range from 350 to 780 nm under identical instrumental conditions as were used to measure the $bR(bR_{LA})$ spectrum (see above). As before, 10 scans were averaged to obtain the final spectrum. (The amount of light exiting the monochromator was significantly less than that required to induce observable photochemistry, even after 10 scans. This prediction was verified by comparing the first and last scans and observing that both were identical within the noise level.)

The photostationary states generated with the three filter assemblies listed above were identical within experimental error. Thus, the 500- and 520-nm photostationary states are identical, an observation that is in agreement with the observations of Hurley and Ebrey.[10] (Our 77 K bR and 500-nm photostationary-state spectra appear very similar to the corresponding spectra obtained by Hurley and Ebrey[10] and Lozier and Niederberger.[17] Our generated K spectrum, however, differs from a majority of those reported previously for reasons outlined below.)

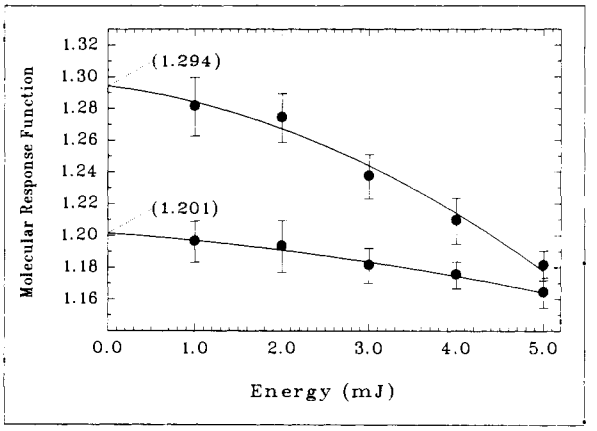

Figure 2. Effect of laser pulse energy on the molecular response functions (Γ) measured for experiment 2 (λ_{exc} = 699 nm, upper curve extrapolating to $\Gamma = 1.294 \pm 0.033$) and for experiment 3 (λ_{exc} = 643 nm, lower curve extrapolating to $\Gamma = 1.201 \pm 0.024$). At higher pulse energies, a larger fraction of the molecules absorbs radiation from the excitation pulse which results in the formation of photoproduct which subsequently absorbs radiation. Thus, as pulse energy increases, Γ approaches unity, the value measured for a photostationary state. These saturation effects are eliminated from biasing the experimental results by fitting the data to a quadratic function and extrapolating to zero pulse energy (see Appendix). The data are from Table II of ref 9.

After the photostationary-state data were collected, the bR spectrum was regenerated according to procedures identical with those used to generate the 500- and 520-nm photostationary states with the exception that a cutoff filter which passes radiation above 620 nm (Corning 2-59, Corning Glass Works, Science Products Division, Corning, NY) was used to preferentially excite only K. The resulting $\lambda > 620$ nm photostationary state has an absorption spectrum equivalent to that of bR and, for the purposes of this investigation, is considered pure bR. Because additional sample cracking occurs during the experiment, we used the final $\lambda > 620$ nm spectrum to correct for base-line drift. Finally, all spectra were referenced and corrected approximately for background protein scattering by use of a sample of chromophore-extracted bleached vertebrate opsin, dissolved in identical solvent and adjusted in concentration so that the 280-nm aromatic amino acid band had the same optical density as the similar band observed for bR. Our PSS-bR difference spectrum is more reliable in the 350–450-nm region, because this spectrum is not dependent

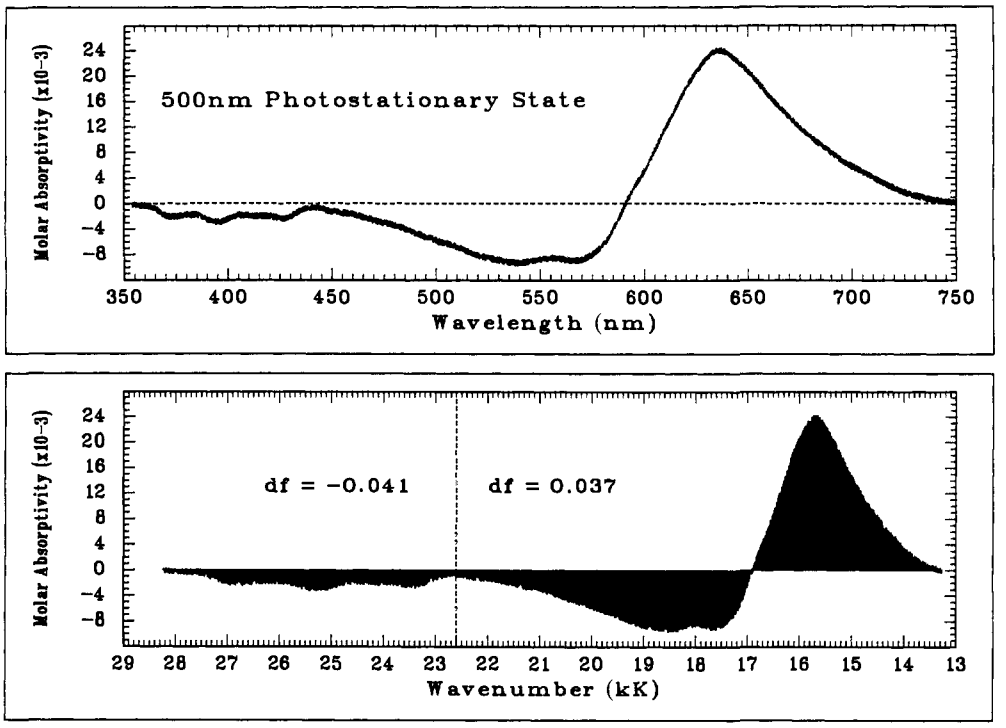

Figure 3. Difference spectrum generated by subtracting the absorption spectrum of light-adapted bacteriorhodopsin from the absorption spectrum of the 500-nm photostationary state. The spectra were measured at 77 K in 2:1 glycerol/H_2O (v/v). The difference spectrum displayed in the top panel is plotted as a function of wavelength, and the spectrum in the bottom panel is plotted as a function of wavenumber ($cm^{-1} \times 10^{-3}$). The changes in oscillator strength associated with the formation of the 500-nm photostationary state are measured for two spectral regions via numerical integration: $\Delta f = -0.041$ (integrated from 22 600 to 28 300 cm^{-1}) and $\Delta f = 0.037$ (integrated from 13 300 to 22 600 cm^{-1}).

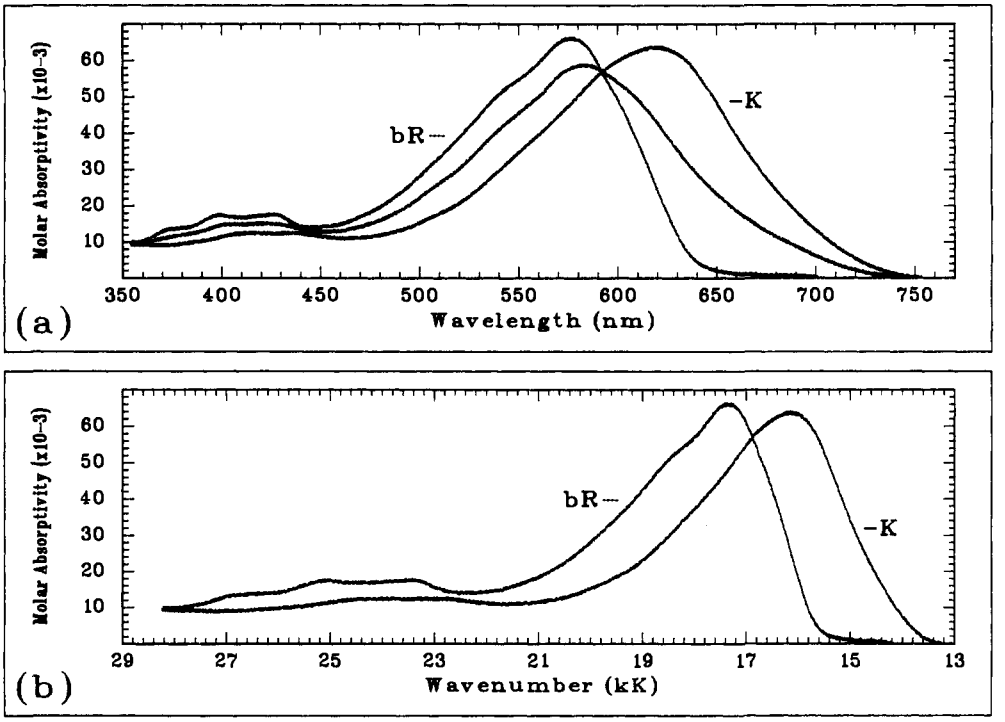

Figure 4. Absorption spectra of bR, K, and the 500-nm photostationary state at 77 K in 2:1 glycerol/H_2O (v/v) are plotted as a function of wavelength in (a). The absorption spectra of bR and K are plotted as a function of wavenumber ($cm^{-1} \times 10^{-3}$) in (b). The absorption spectrum of K is calculated by assuming that the 500-nm photostationary has a molar distribution of 54% bR and 46% K (see text).

upon the assignment of the protein background spectrum.

Photocalorimetric data regression studies were carried out with the raw experimental data measured previously by Birge and Cooper, and the interested reader is referred to ref 9 for the experimental details. Of relevance to the present investigation are the procedures of data analysis and the dependence of these procedures on various assumptions concerning the photochemistry and spectroscopy of bR and K.

Photocalorimetry based on the use of the photostationary state as an internal standard is not capable of determining Φ_1, Φ_2, and ΔH_{12} simultaneously.[9] This limitation requires that one of the above three parameters be assigned on the basis of a separate experimental measurement in order to determine the other two. However, the photocalorimetry data can be used to determine $\Delta H_{12}(\Phi_1)$ and Φ_1/Φ_2 and, in conjunction with the appropriate photostationary-state spectral data, to determine the mole fraction of K in the photostationary state (χ_K^{500}) and therefore the absorption spectrum of K.

The pulsed laser photocalorimeter measures a molecular response function Γ_λ

$$\Gamma_\lambda = \alpha^{\lambda_{prep}}_{\lambda_{exc}}\left(1 - \Phi_1\frac{\Delta H_{12}}{\Delta H_{photon}}\right) + (1 - \alpha^{\lambda_{prep}}_{\lambda_{exc}})\left(1 + \Phi_2\frac{\Delta H_{12}}{\Delta H_{photon}}\right) \quad (2)$$

where Φ_1, Φ_2, and ΔH_{12} are defined in eq 1, ΔH_{photon} is the energy per mole of the monochromatic pulsed laser excitation of wavelength λ

$$\Delta H_{photon} = 28\,590 \text{ kcal mol}^{-1}/\lambda \text{ (nm)} \quad (3)$$

and $\alpha^{\lambda_{prep}}_{\lambda_{exc}}$ is the photochemical partition function

$$\alpha^{\lambda_{prep}}_{\lambda_{exc}} = [bR]\epsilon^{\lambda_{exc}}_{bR}/([bR]\epsilon^{\lambda_{exc}}_{bR} + [K]\epsilon^{\lambda_{exc}}_{K}) \quad (4)$$

where ϵ^{λ}_{bR} is the molar absorptivity of light-adapted bR at the excitation wavelength, λ_{exc}, and [bR] is the concentration of bR appropriate to the initial conditions or preparation wavelength, λ_{prep}. The terms ϵ^{λ}_{K} and [K] are defined similarly for K. The inclusion of the preparation wavelength in defining the photochemical partition function is required because many of the experiments are carried out on a photostationary-state mixture which is produced via preirradiation of the sample at λ_{prep}.[9]

Three experiments were carried out to measure the photocalorimetric response of bR and K at 77 K. These three experiments have been described previously,[9] but in this paper we have reassigned the molecular response functions for two of the three experiments. The key difference between the current approach and that used previously by Birge and Cooper[9] is the present use of second-order polynomial regression to assign Γ_λ for the two experiments carried out on the 500-nm photostationary state (see Appendix). This approach was adopted because of the importance of assigning statistically well-defined values of the molecular response function to the analysis of Φ_1/Φ_2 and χ_K^{500}. As we discuss below, however, our revised procedures do not have a significant effect on the calculation of energy storage, and the previous measurement in ref 9 (ΔH_{12} = 15.8 ± 2.5 kcal mol^{-1}) is increased only slightly in this reevaluation.

Experiment 1 was carried out on pure bR maintained via preparative irradiation at wavelengths greater than $\lambda > 620$ nm. Accordingly, [bR] ≫ [K], and pulsed laser excitation at 565 nm (ΔH_{photon} = 50.6 kcal mol^{-1}) will excite only bR so that $\alpha_{565}^{\geq 620} \sim 1$. The molecular response function was measured to be $\Gamma_{565} = 0.907 \pm 0.021$ and was observed to be independent of laser pulse energy in the region 1–5 mJ/pulse.

Experiment 2 was carried out on the 500-nm photostationary state (PSS_{500}), which is a mixture of bR and K. The composition of the 500-nm PSS is a subject of this investigation, and thus $\alpha^{500}_{\lambda_{exc}}$ will remain undefined at present. Pulsed laser excitation at 699 nm (ΔH_{photon} = 40.9 kcal mol^{-1}) was used in order to maximize the probability of selectively exciting K and not exciting bR ($\alpha_{699}^{500} \sim 0$). The molecular response function was observed to exhibit a laser pulse energy dependence which upon second-order polynomial regression extrapolates to $\Gamma_{699}(PSS_{500}) = 1.294 \pm 0.033$ (see Figure 2).

Experiment 3 was identical with experiment 2 except that pulsed laser excitation at 643 nm (ΔH_{photon} = 44.5 kcal mol^{-1}) was used in order to excite a mixed photoreaction. The molecular response function was observed to exhibit a laser pulse energy dependence which upon second-order polynomial regression extrapolates to $\Gamma_{643}(PSS_{500}) = 1.201 \pm 0.024$ (see Figure 2).

Results and Discussion

Two of the three photocalorimetry experiments were carried out with 500-nm irradiation to prepare a photostationary-state mixture of bR and K in order to maximize the relative amount of K in the solution. (Previous studies have indicated that the concentration ratio, [K]/[bR], at 77 K is maximum for photostationary mixtures prepared with 500–520-nm irradiation.[10]) Knowledge of the photostationary state composition is critical to an analysis of the 643-nm excitation data (experiment 3) because both bR and K absorb meaningful fractions of the incident irradiation, and hence initial concentrations, and molar absorptivities at the exciting wavelength (643 nm) must be known in order to assign α_{643}^{500}.

Photostationary-State Analysis. Deconvolution of the photostationary-state spectrum into individual component spectra required assignment of both Φ_1/Φ_2 and ϵ_K^{500}. The former cannot be assigned without analysis of the photocalorimetry data, and the latter requires assignment of the mole fraction of K, χ_K^{500}, present in the photostationary-state mixture:

$$\chi_K^{500} = \frac{[K]}{[K] + [bR]} \quad (5)$$

Table II. Photophysical Properties of Light-Adapted Bacteriorhodopsin at 77 K Based on Analysis of 500-nm Photostationary-State Data as a Function of Φ_1/Φ_2

Φ_1/Φ_2[a]	χ_K[b]	ϵ_K^{500nm}[c]	λ_{max}(K)[d]	$f[\lambda_{max}(K)]$[e]	α_{643}^{500}[f]	α_{699}^{500}[f]
0.05	0.250	4.219	633.5	1.019	0.099	0.006
0.10	0.283	6.660	632.4	1.003	0.094	0.006
0.20	0.342	10.457	629.6	0.980	0.086	0.005
0.30	0.393	13.075	626.2	0.964	0.080	0.005
0.40	0.437	14.808	622.4	0.953	0.074	0.005
0.41	0.441	14.943	622.0	0.952	0.073	0.005
0.42	0.445	15.072	621.5	0.951	0.073	0.004
0.43	0.449	15.194	621.1	0.951	0.072	0.004
0.44	0.453	15.312	620.7	0.950	0.072	0.004
0.45	**0.457**	**15.423**	**620.3**	**0.949**	**0.071**	**0.004**
0.46	0.460	15.530	619.9	0.949	0.071	0.004
0.47	0.464	15.631	619.5	0.948	0.070	0.004
0.48	0.468	15.728	619.1	0.947	0.070	0.004
0.49	0.471	15.820	618.6	0.947	0.069	0.004
0.50	0.475	15.908	618.2	0.946	0.069	0.004
0.55	0.492	16.289	616.1	0.944	0.067	0.004
0.60	0.507	16.589	614.0	0.942	0.064	0.004
0.70	0.536	17.025	609.8	0.939	0.061	0.004
0.80	0.561	17.353	605.7	0.937	0.057	0.004
0.90	0.584	17.670	602.0	0.935	0.054	0.003
1.00	0.605	18.035	598.7	0.933	0.052	0.003

[a] Ratio of the forward to reverse quantum yields at 77 K (see eq 1). [b] Mole fraction of K in 500-nm photostationary state based on value of Φ_1/Φ_2 shown in left-hand column. [c] Molar absorptivity of K at 500 nm and 77 K based on analysis of 500-nm photostationary state assuming the value of Φ_1/Φ_2 shown in left-hand column. Values are in mM^{-1} cm^{-1}. [d] Absorption maximum of K in nm at 77 K based on analysis of 500-nm photostationary state assuming the value of Φ_1/Φ_2 shown in left-hand column. [e] Oscillator strength of the λ_{max} absorption band of K at 77 K based on analysis of 500-nm photostationary state assuming the value of Φ_1/Φ_2 shown in left-hand column. [f] Values of the photochemical partition function $\alpha^{500}_{\lambda_{exc}}$ at the specified excitation wavelength (subscripted) at 77 K based on analysis of 500-nm photostationary state assuming the value of Φ_1/Φ_2 shown in left-hand column.

Accordingly, a self-consistent approach to the analysis of the spectroscopic and photocalorimetric data is required. We therefore carried out a preliminary analysis on the photostationary-state data under the assumption that χ_K^{500} equaled 0.3. Analysis of the photostationary-state data shown in Figures 3 and 4 yielded the results shown in Table II. The photocalorimetric data were then analyzed according to the procedures outlined below on the basis of the data of Table II for $\chi_K^{500} = 0.3$. This approach produced a value for Φ_1/Φ_2 that could be used to generate a better estimate for χ_K^{500}. The iterative process was continued until convergence was reached, and the viability of the final number was verified by repeating the self-consistence approach with different starting values of χ_K^{500}. Eight iterations were normally required, and a final value of $\chi_K^{500} = 0.46 \pm 0.03$ was obtained regardless of the initial value assumed for the mole fraction. To avoid confusion, we will discuss the following procedures without reference to the intermediate iterative details.

The 500-nm photostationary-state difference spectrum ($\epsilon_K^{500} - \epsilon_{bR}^{500}$) is presented in Figure 3. The relative concentrations of bR and K obey the following relationship:

$$\frac{\Phi_1}{\Phi_2} = \frac{\epsilon_K^{500}}{\epsilon_{bR}^{500}}\frac{[K]}{[bR]} \quad (6)$$

Analysis of the photostationary-state data as a function of Φ_1/Φ_2 yields the results shown in Table II. The iterative analyses of the results shown in Table II along with the photocalorimetric data (see below) indicate that $\Phi_1/\Phi_2 = 0.45 \pm 0.03$. The mole fraction of K in the 500-nm photostationary state is given by the expression

$$\chi_K^{500} = (\Phi_1/\Phi_2)\epsilon_{bR}^{500}/[\epsilon_K^{500} + (\Phi_1/\Phi_2)\epsilon_{bR}^{500}] \quad (7)$$

Solution of this equation as a function of Φ_1/Φ_2 is given in column 2 of Table II and yields $\chi_K^{500} = 0.46 \pm 0.04$ for $\Phi_1/\Phi_2 = 0.45 \pm 0.03$ (the similarity of the two values is fortuitous).

Accordingly, the 500-nm, 77 K photostationary state contains 46% K and 54% bR. The absorption spectrum of K at 77 K can be calculated with the expression

$$\epsilon_K^\lambda = [\epsilon_{PSS}^\lambda - (1 - \chi_K^{500})\epsilon_{bR}^\lambda]/\chi_K^{500} \quad (8)$$

and the results of this analysis are shown in Figure 4. The 77 K absorption spectrum of K has a λ_{max} at 620 nm, and the λ_{max} band has an oscillator strength of 0.95, which is larger than the analogous parameter measured for bR ($f = 0.87$). This observation is consistent with the 500-nm photostationary-state difference spectrum (Figure 3) which indicates that formation of a mixture of bR and K increases the system oscillator strength in the long-wavelength band system ($\Delta f = 0.037$ for the 13 000–22 600-cm^{-1} region). The observation that K has a larger λ_{max} band oscillator strength than bR has potential implications for the nature of the primary photochemical process. This issue will be explored in greater detail below.

Photocalorimetric Analysis. The three experiments described under Experimental Section can be reduced to a set of three equations in three unknowns (Φ_1, Φ_2, and ΔH_{12}) by substituting the appropriate values of ΔH_{photon} and Γ_λ into eq 2:

$$0.907 = \alpha_{565}^{>620}(1 - \Phi_1\Delta H_{12}/50.6) + (1 - \alpha_{565}^{>620})(1 + \Phi_2\Delta H_{12}/50.6) \quad (9)$$

$$1.294 = \alpha_{699}^{500}(1 - \Phi_1\Delta H_{12}/40.9) + (1 - \alpha_{699}^{500})(1 + \Phi_2\Delta H_{12}/40.9) \quad (10)$$

$$1.201 = \alpha_{643}^{500}(1 - \Phi_1\Delta H_{12}/44.5) + (1 - \alpha_{643}^{500})(1 + \Phi_2\Delta H_{12}/44.5) \quad (11)$$

Numbers in italics in eq 9–11 are in kcal mol^{-1}. Prior to evaluation of these three equations by a simultaneous regression analysis, it is useful to carry out a simple analysis of eq 9 and 10 in order to demonstrate the invariance of the quantum yield ratio, Φ_1/Φ_2, to changes in the independent variables, Φ_1, Φ_2, and ΔH_{12}.

Irradiation of a mixture of bR and K at wavelengths greater than 620 nm produces >97% bR, and hence, $\alpha_{565}^{>620} \sim 1$. Equation 9 reduces to

$$\Phi_1 \cong 4.7 \text{ kcal mol}^{-1}/\Delta H_{12} \quad (12)$$

Similarly, when a 500-nm photostationary-state mixture of bR and K is excited at a wavelength of 699 nm, the K intermediate will absorb a majority of the radiation because the absorptivity of bR is significantly smaller than the absorptivity of K at this wavelength ($\epsilon_{bR}^{699} \cong 250$ M^{-1} cm^{-1}; $\epsilon_K^{699} \cong 13\,500$ M^{-1} cm^{-1}; see Figure 4). Thus, $\alpha_{699}^{500} \sim 0$, and eq 10 reduces to

$$\Phi_2 \cong 12 \text{ kcal mol}^{-1}/\Delta H_{12} \quad (13)$$

Dividing eq 12 by eq 13 leads to an approximate value for the quantum yield ratio:

$$\Phi_1/\Phi_2 \cong 0.4 \quad (14)$$

The above value is approximate because we have ignored contributions from eq 11 as well as residual effects associated with nonzero values for α_{699}^{500} and for $1 - \alpha_{565}^{>620}$. Nevertheless, the above analysis demonstrates the application of photocalorimetry to the assignment of Φ_1/Φ_2.

We now turn to a full-weighted least-squares regression analysis of eq 9–11 in order to determine more accurately values for Φ_2, $\Phi_1 + \Phi_2$, and ΔH_{12} as a function of Φ_1. These calculations make use of the photostationary-state spectroscopic data presented in Figure 3 and the absorption spectrum of bR shown in Figure 4 to assign $\alpha_{565}^{>620}$, α_{699}^{500}, and α_{643}^{500} as a function of Φ_1 prior to carrying out the regression analysis for each value of Φ_1. Our methods and procedures of carrying out the regression analysis are identical with those described in ref 9 except for the fact that the spectra of Figure 4 are used to assign $\alpha_{565}^{>620}$, α_{699}^{500}, and α_{643}^{500} and eq 9–11 are used (rather than eq 11–13 from ref 9). Thus the assumptions that were used in deriving eq 12–14 are not adopted. The results of our regression analysis are presented in Table III.

The data presented in Table III lead to important conclusions with regard to the primary quantum efficiencies associated with the bR and K photoequilibrium at 77 K. First, and most important, the ratio Φ_1/Φ_2 is invariant to changes in Φ_1 in the range $\Phi_1 = 0.19$ to $\Phi_1 = 0.96$. Accordingly, our experimental studies provide a reliable assignment of the ratio of $\Phi_1/\Phi_2 = 0.45 \pm 0.03$, regardless of reasonable assignment of Φ_1. The ratio determined from the photocalorimetry data is higher than those values reported by Goldschmidt et al.,[11,12] Becher and Ebrey,[13] and Dioumaev et al.[19] and slightly lower than the value reported by Hurley and Ebrey[10] (see Table I). Our results indicate that Φ_1 must be less than or equal to 0.48 at 77 K. It should be reemphasized, however, that our photocalorimetry experiments do not provide an independent measurement of Φ_1 in the absence of an independent measurement of Φ_2 or ΔH_{12}. Nevertheless, assignment of an upper limit to Φ_1 provides an important perspective on the literature controversy as discussed below.

Values of Φ_2 and $\Phi_1 + \Phi_2$ as a function of Φ_1 are also presented in Table III. Although the error ranges associated with these assignments are significant, it is clear that values of Φ_1 equal to or greater than 0.48 lead to unrealistic values for Φ_2, a result that follows directly from the invariance of $\Phi_1/\Phi_2 = 0.45 \pm 0.03$. Our results constrain the sum $\Phi_1 + \Phi_2$ to values less than or equal to 1.48, but it should be noted that this result is not obvious from the error ranges listed for this sum in Table III. The error ranges shown in Table III are based on standard deviations for the indicated parameters, but a global analysis of the data based on the constraint that $\Phi_2 \leq 1$ (a constraint not implicit in the least-squares regression analysis) requires that $\Phi_1 + \Phi_2 \leq 1.48$.

Possible Origins of the Variations in Measured Values of the Primary Quantum Yield. The values reported for Φ_1 in Table I vary from 0.25 to 0.79, a range roughly 5 times larger than that anticipated on the basis of experimental error. Before the possible molecular origins of the experimental range are analyzed, it is appropriate to consider the possibility that an inner-filter effect is responsible for generating anomalous quantum yield measurements. Kouyama et al. have examined the influence of the N intermediate on the bacteriorhodopsin photocycle.[4a] These investigators propose that the N intermediate has a major absorption maximum between 550 and 560 nm and is photoactive. At high pH and high light intensity, the overall photoreaction of bacteriorhodopsin may be approximated by the multiphoton cycle

$$bR \xrightarrow{h\nu} K \rightarrow L \rightarrow M \rightarrow N \xrightarrow{h\nu} ({}^NL \Leftrightarrow {}^NM) \rightarrow bR$$

whereas at neutral pH and low light intensity it can be described by the one-photon cycle

$$bR \xrightarrow{h\nu} K \rightarrow L \rightarrow M \rightarrow N \rightarrow O \rightarrow bR$$

Thus, the above two schemes could account for anomalies in quantum yield measurements at ambient temperatures involving the observation of M. For example, the presence of the two-photon cycle would artificially decrease the measured quantum yield of M formation by up to half. Thus, if we assume $\Phi_1 \sim 0.6$, a continuous-wave experimental measurement at high pH and high light intensity could yield ~0.3, because roughly half of the photons absorbed would be absorbed by N, which has an absorption spectrum very similar to that of bR. While it is possible that some of the measurements reported in Table I might have been affected by this inner-filter effect, a majority of the measurements reported in Table I do not. Thus, we must seek alternative explanations.

A cursory examination of Table I suggests that environment and/or temperature may be responsible for producing the large variations in experimental values. While it is true that all of the measurements resulting in values of $\Phi_1 \geq 0.6$ were carried out at ambient temperature, three ambient-temperature measurements yielded values in the range 0.25–0.31. Thus, while temperature may represent an important variable, it is not uniquely responsible for generating the large differences in Φ_1. A second possibility is environment. Two of the three ambient-temperature measurements generating values of $\Phi_1 > 0.6$ were carried out by

Table III. Assignments of Φ_1/Φ_2, $\Phi_2(\Phi_1)$, $[\Phi_1 + \Phi_2](\Phi_1)$, and $\Delta H_{12}(\Phi_1)$ Based on Global Optimization of the Photocalorimetry Measurements at 77 K[a]

Φ_1[b]	$\Phi_2(\Phi_1)$	$[\Phi_1 + \Phi_2](\Phi_1)$	$\Delta H_{12}(\Phi_1)$ (kcal mol^{-1})
0.20	0.455 ± 0.106	0.655 ± 0.152	25.36 ± 5.79
0.25	0.569 ± 0.132	0.819 ± 0.190	20.29 ± 4.63
0.30	0.683 ± 0.159	0.983 ± 0.228	16.91 ± 3.86
0.35	0.797 ± 0.185	1.147 ± 0.266	14.49 ± 3.31
0.40	0.911 ± 0.211	1.311 ± 0.304	12.68 ± 2.90
0.45	1.025 ± 0.238	1.475 ± 0.342	11.27 ± 2.57
0.50	*1.139 ± 0.264*	*1.639 ± 0.380*	*10.14 ± 2.32*[c]
0.55	*1.252 ± 0.291*	*1.802 ± 0.418*	*9.22 ± 2.11*
0.60	*1.366 ± 0.317*	*1.966 ± 0.456*	*8.45 ± 1.93*
0.65	*1.480 ± 0.344*	*2.130 ± 0.494*	*7.80 ± 1.78*
0.70	*1.594 ± 0.370*	*2.294 ± 0.532*	*7.25 ± 1.65*
0.75	*1.708 ± 0.396*	*2.458 ± 0.570*	*6.76 ± 1.54*
0.85	*1.935 ± 0.449*	*2.785 ± 0.646*	*5.97 ± 1.36*
0.95	*2.163 ± 0.502*	*3.113 ± 0.723*	*5.34 ± 1.22*

$\Phi_1/\Phi_2 = 0.445 \pm 0.031$ ($0.19 < \Phi_1 < 0.96$; 77 K)

[a] The results presented in this table differ slightly from those presented for the restricted range of $\Phi_1 = 0.24$–0.38 in Table III of ref 9, because the present analysis uses least-squares regression techniques to assign the molecular response function for experiments 2 and 3 (see Figure 2 and the Experimental Section). [b] Values of the primary quantum yield, Φ_1, are assumed, and the values of the remaining parameters listed in the same row are optimized via least-squares regression on the basis of this assignment. Note that values of Φ_1 greater than 0.48 are suspect, because such values result in a calculated value of $\Phi_2(\Phi_1)$ that is larger than unity (which is a physical impossibility) on the basis of the regression assignment of the quantum yield ratio, $\Phi_1/\Phi_2 = 0.445 \pm 0.031$. [c] Values of ΔH_{12} predicted for $\Phi_1 > 0.48$ are not reliable, because the global least-squares regression was not constrained to prevent Φ_2 from exceeding unity (see text for details).

measuring the formation of M in high-salt, ether solution. Ether is known to increase the lifetime of the M intermediate,[13,16] although the mechanism is not understood. It is also known that salt concentration has a dramatic effect on the quantum yield of proton translocation.[5,6] Finally, recent investigations suggest that the nature of the photocycle is dramatically affected by pH.[22,23] These latter studies suggest that there are at least two independent photocycles for light-adapted bacteriorhodopsin, one which is responsible for generating M_{fast} and a second which is responsible for generating M_{slow}. A third photocycle may be responsible for generating the recently observed intermediate called R.[23,24] Thus, a distribution of photocycles may exist. We suggest the possibility that different photocycles may exhibit different primary quantum yields. Solvent, temperature, ionic strength, and pH may affect the distribution of these photocycles in a complex way that remains to be explored in detail. We also suggest the possibility that photochemistry, rather than environment, may be a key selector of photocycle (see below). This proposal is based on the observation that *all* direct experimental measurements on Φ_1 yield values greater than or equal to 0.6, while *all* photostationary-state measurements on Φ_1 yield values less than or equal to 0.33. This issue will be explored in greater detail below. First, we will explore some possible molecular origins for different primary quantum yields from the same protein.

The notion that two distinct forms of light-adapted bacteriorhodopsin are present, each with a characteristic photocycle that differs with respect to the primary photochemical quantum yield, gains further support from two observations, one experimental and the second theoretical. The experimental observation is based on an analysis of the measured values of Φ_1 reported in Table I. This tabulation indicates that all of the direct experimental measurements fall into one of two categories—those that predict $\Phi_1 \approx 0.3$ or below and those that predict $\Phi_1 \approx 0.6$ or above. No experimental measurements fall into the large intermediate range of 0.34–0.59. If experimental uncertainty were the dominant source of the discrepancies in the measured quantum yields, one would predict that a majority of the measurements would fall into this intermediate range in contrast to none at all. Thus, the experimental data support the concept that two photocycles are present and that experimental conditions tend to preferentially select one or the other.

The theoretical evidence in support of this concept is obtained by a closer analysis of the molecular dynamics calculations reported in ref 25. These calculations, which were based on the theoretical procedures described in ref 26, predict complex dynamics and biphasic repopulation of the ground state following excitation of bR (see Figure 5). The key observation is that roughly one-third of the excited molecules are trapped in an excited-state potential well and decay back to the ground state via nondynamic processes. The simulations reported in ref 25 predict that this S_1* potential well has a 13-transoid minimum so that decay of those species trapped in this well preferentially regenerates bR. However, it should be noted that the ground-state conformation of bR (hereafter referred to as bR_1) assumed in the calculations was optimized so that the optical and photocalorimetric data at 77 K were reproduced (see Figure 5). If we allow for a smaller amount of energy storage in the primary event and arbitrarily move the entire chromophore away from the counterion by rotation about the β–γ lysine bond (see Figue 1 of ref 25), thereby decreasing electrostatic stabilization of the all-trans chromophore, the potential well in the first excited singlet state shifts to a 13-cisoid conformation (see Figure 5). We will refer to this ground-state geometry as bR_2. The molecular dynamics calculations predict that roughly one-third of the bR_2 molecules excited into the lowest singlet state are trapped in the 13-cisoid S_1* potential well and preferentially decay to form product (J or K). (For the purposes of this discussion, we are treating J and K as similar species with respect to chromophore geometry with both species possessing ground-state 13-cis geometries. The possibility that J is an excited-state species, however, has been proposed.[27]) Accordingly, our calculations predict that a small

(22) Hanamoto, J. H.; Dupois, D.; El-Sayed, M. A. *Proc. Natl. Acad. Sci. U.S.A.* **1984**, *81*, 7083–7087.
(23) Dancshazy, Zs.; Govindjee, R.; Ebrey, T. G. *Proc. Natl. Acad. Sci. U.S.A.* **1988**, *85*, 6358–6361.
(24) Drachev, L. A.; Kaulen, A. D.; Skulachev, V. P.; Zorina, V. V. *FEBS Lett.* **1986**, *209*, 316–320.
(25) Birge, R. R.; Findsen, L. A.; Pierce, B. M. *J. Am. Chem. Soc.* **1987**, *109*, 5041–5043.
(26) Birge, R. R.; Hubbard, L. M. *J. Am. Chem. Soc.* **1980**, *102*, 2195–2205. Birge, R. R.; Hubbard, L. M. *Biophys. J.* **1981**, *34*, 517–534. Birge, R. R. In *Biological Events Probed by Ultrafast Laser Spectroscopy*; Alfano, R. R., Ed.; Academic Press: New York, 1982; pp 299–317.
(27) A majority of researchers have concluded that the first photoproduct trapped at 77 K is K, and not its precursor J (see ref 2, 9, 10, and 17). A key observation in support of this conclusion is that the transient absorption maximum of J at ambient temperature ($\lambda_{max} \sim 625$ nm) is red shifted relative to the absorption maximum of the photoproduct trapped at 77 K ($\lambda_{max} \sim 620$ nm). All the other intermediates, as well as bR, have ambient temperature maxima blue shifted ~10 nm relative to the corresponding absorption maxima observed at 77 K. Analysis of the molecular dynamics calculations presented in ref 25 suggests the possibility that J might be an excited-state species. The key element of this proposal is the observation that roughly one-third of the excited state species are trapped in an S_1* potential well and that the electronic absorption spectrum associated with these metastable species (principally $S_1 \rightarrow S_4, S_5$) is predicted to occur at ~650 nm, very close to the λ_{max} absorption band of the J intermediate (see ref 25 for details). This assignment has been criticized by Mathies and co-workers,[28] who have carried out femtosecond optical measurements on the primary event of bR. These investigators observe the appearance of the J absorption signal synchronous with the filling-in of the (absorption) hole at 568 nm.[28] These features, however, are consistent with an excited-state J species that is formed on the same time scale as the re-formation of bR associated with dynamic processes. However, our model predicts that for bR_1 systems longer time decay of J will increase bR population, and hence, the signal at 580 nm should increase synchronously with decay of J as well. Alternatively, the model based on bR_2 dynamics (see Figure 5) predicts that decay of J will increase K population, and hence, the signal at ~600 nm will increase synchronously with decay of J. Our calculations predict that the decay of J back to the ground state may have a small radiative component which is observable potentially as a broad fluorescence band at ~1300 Å. Alternatively, if it were possible to trap J at extremely low temperatures and verify that it has a vibrational spectrum differing from that of K, our proposal that J is an excited-state species would be proven wrong. It should be noted, however, that the assignment of J as a ground-state or as an excited-state species is not of importance to the present investigation. As noted above, this spectroscopic precursor is not trapped under the experimental conditions used here.
(28) Mathies, R. A.; Brito Cruz, C. H.; Pollard, W. T.; Shank, C. V. *Science* **1988**, *240*, 777.

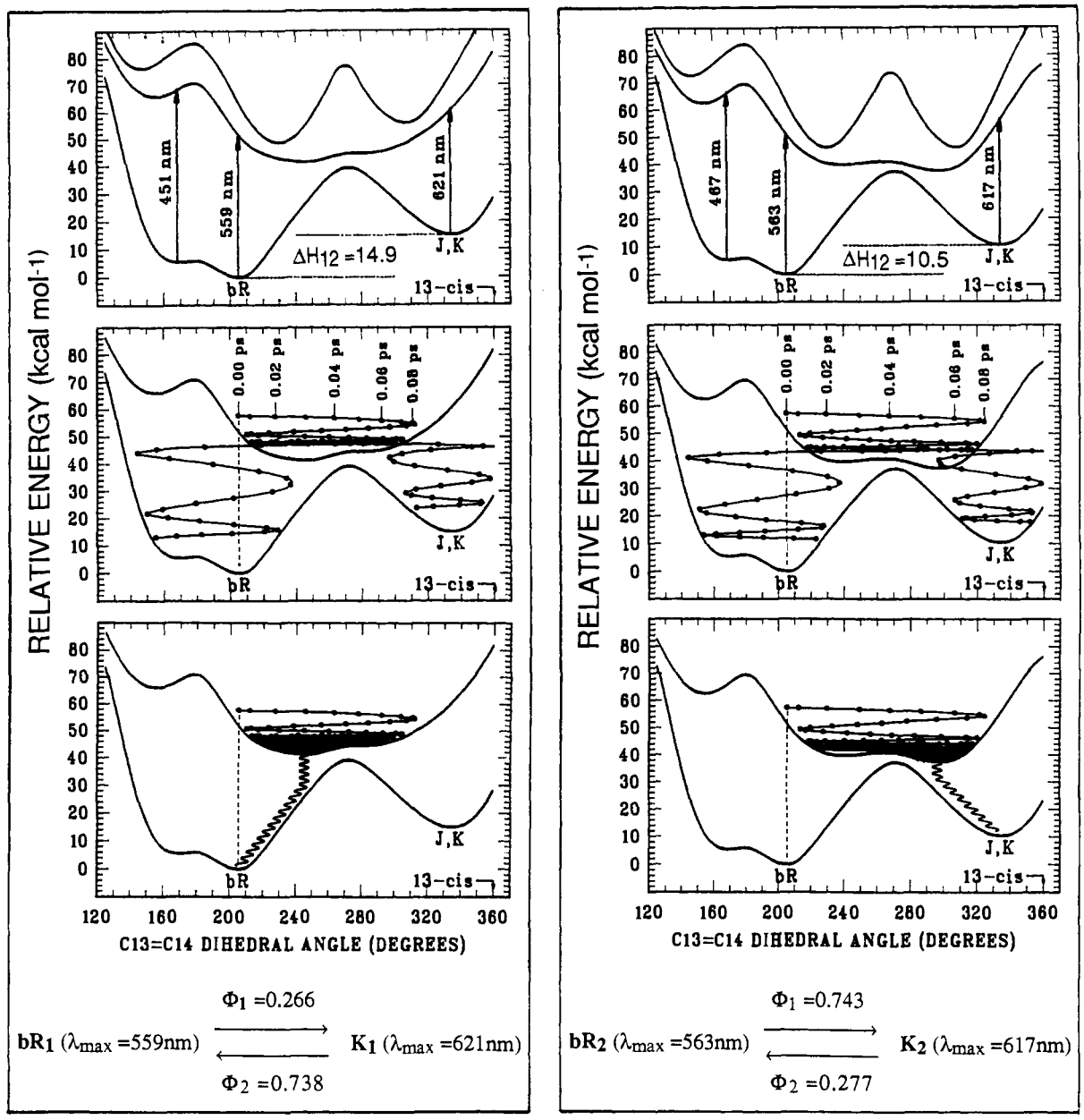

Figure 5. Molecular dynamics of the primary photochemical transformation of light-adapted bacteriorhodopsin based on two different models of the binding site. The calculations shown in the left rectangle are reproduced from ref 25 and are based on the binding site model shown in Figure 1a,b of ref 25. Roughly one-third of the excited molecules are trapped in an excited-state potential well and decay back to the ground state via nondynamic processes. The simulations predict that this S_1* potential well has a 13-transoid minimum so that decay of those species trapped in this well preferentially regenerates bR. The ground-state conformation of bR (referred to as bR_1) assumed in the calculations shown on the left was optimized to reproduce as accurately as possible the optical and photocalorimetric data at 77 K. The calculations shown in the rectangle at right were carried out by allowing for a smaller amount of energy storage in the primary event and arbitrarily moving the entire chromophore away from the counterion by rotation about the β–γ lysine bond. This change decreases electrostatic stabilization of the all-trans chromophore and shifts the S_1* potential well to a 13-cisoid conformation. We refer to this geometry as bR_2. The molecular dynamics calculations predict that roughly one-third of the bR_2 molecules excited into the lowest singlet state are trapped in this S_1* potential well and preferentially decay to form product (J or K). The calculations predict that a small change in ground-state geometry produces a dramatic increase in the primary quantum yield [$\Phi_1(bR_1) = 0.266$; $\Phi_1(bR_2) = 0.743$]. Because the probability of coupling into the ground state is relatively low for each trajectory (average crossing probability is less than 10% for the first 10 passes over the orthogonal crossing region), the quantum yield sums are very close to unity for both geometries [$(\Phi_1 + \Phi_2)(bR_1) = 1.004$; $(\Phi_1 + \Phi_2)(bR_2) = 1.02$]. Although the bR_2 geometry is calculated to have a higher chromophore–counterion energy ($\sim$2 kcal mol^{-1}) relative to the bR_1 geometry (based on the binding site model of ref 25), the bR_2 geometry may be more stable when the entire protein energy is taken into account.

change in ground-state binding site geometry produces a dramatic increase in the primary quantum yield [$\Phi_1(bR_1) = 0.266$; $\Phi_1(bR_2) = 0.743$; see Figure 5]. Although the bR_2 geometry is calculated to have a higher chromophore–counterion energy ($\sim$2 kcal mol^{-1}) relative to the bR_1 geometry (based on our model of the binding site), the latter geometry may be more stable under certain environmental conditions when the entire protein energy is taken into account. Furthermore, it is possible that a change in the ionization state of a group on the apoprotein, rather than a change in the chromophore–counterion geometry, is responsible for transforming bR_1 to bR_2. The recent studies of El-Sayed and co-workers[22] provide support for this alternative hypothesis. These investigators proposed that the biphasic kinetics observed in the formation of M are associated with two different chromophore environments provided by the apoprotein.[22] They proposed further that the two forms are alternately populated depending upon the ionization state of an apoprotein moiety with a pK near 9.6. A third possibility, which gains support from an analysis of the data shown in Table I, is that photochemistry, rather than environment, may be the primary mechanism of selecting bR_1 versus bR_2. As

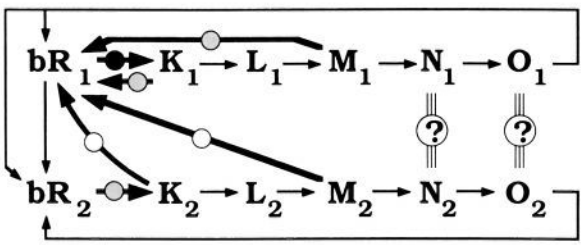

Figure 6. A dual photocycle model of bacteriorhodopsin which rationalizes the experimental observation that *all* direct measurements on Φ_1 yield values greater than or equal to 0.6, while *all* photostationary-state measurements on Φ_1 yield values less than or equal to 0.33. The thick arrows indicate photochemical transformations, and the quantum efficiency of the photochemical transformations are indicated by circles: white (Φ unknown), black ($\Phi \sim 0.3$), grey ($\Phi \sim 0.6$). Accordingly, $bR_1 \xrightarrow{\sim 0.3} K_1$, $bR_2 \xrightarrow{\sim 0.6} K_2$, $K_2 \xrightarrow{?} bR_1$, $K_1 \xrightarrow{\sim 0.6} bR_1$, $M_1 \xrightarrow{\sim 0.6} bR_1$, etc. The thin arrows indicate thermal transformations. Thus, the bR_2 photocycle, which has the higher primary quantum yield, is the thermally more stable. Direct measurements will yield high values for Φ_1, because the $bR_2 \xrightarrow{h\nu} K_2$ photoreaction will be selected. However, the back-reaction is not $K_2 \xrightarrow{h\nu} bR_2$ but rather $K_2 \xrightarrow{h\nu} bR_1$. Subsequent photochemistry will take place within the bR_1 photocycle, which will select the $bR_1 \xrightarrow{h\nu} K_1$ reaction and yield a lower primary quantum yield. Because the reverse photoreaction from K_1 also selects bR_1, all photostationary measurements will measure the $bR_1 \xrightarrow{h\nu} K_1$ quantum yield, which is ~0.3. It is possible that at some stage in the photocycles the intermediates of the two photocycles are equivalent (i.e., $L_1 \equiv L_2$, $M_1 \equiv M_2$, $N_1 \equiv N_2$, and $O_1 \equiv O_2$). Thus, bR_2 could be formed via thermal relaxation of bR_1 or directly via $O_1 \equiv O_2$.

noted above, *all* direct experimental measurements on Φ_1 yield values greater than or equal to 0.6, while *all* photostationary-state measurements on Φ_1 yield values less than or equal to 0.33. This observation suggests a dual photocycle system as depicted in Figure 6. The thick arrows in this figure indicate photochemical transformations while the thin arrows indicate thermal transformations. Thus, the bR_2 photocycle, which has the higher primary quantum yield, is the thermally more stable. Direct measurements will yield high values for Φ_1, because the $bR_2 \xrightarrow{h\nu} K_2$ photoreaction will be selected. However, the back-reaction is not $K_2 \xrightarrow{h\nu} bR_2$ but rather $K_2 \xrightarrow{h\nu} bR_1$. Subsequent photochemistry will take place within the bR_1 photocycle, which will select the $bR_1 \xrightarrow{h\nu} K_1$ reaction and yield a lower primary quantum yield. Because the reverse photoreaction from K_1 also selects bR_1, all photostationary measurements will measure the $bR_1 \xrightarrow{h\nu} K_1$ quantum yield, which is ~0.3.

Regardless of which of the above alternatives is assigned as the dominant mechanism for selecting bR_1 versus bR_2, the key proposal is that a small change in protein geometry or binding site electrostatic environment can have a dramatic effect on the primary quantum yield. We should note, however, that we view the molecular dynamics calculations presented in Figure 5 as illustrative rather than quantitatively relevant. In the absence of a detailed knowledge of the protein binding site geometry and the location of nearby ionizable protein residues, a more definitive analysis of how the protein affects the population of bR_1 versus bR_2, or the mechanistic details associated with the photocycles of these two species, is not possible.

Absorption Spectrum and λ_{max} Oscillator Strength of K. As noted above, our photocalorimetry and photostationary-state analyses predict that the mole fraction of K in the 500-nm photostationary-state mixture, χ_K^{500}, is equal to 0.46 ± 0.04. This value is larger than two of the previous measurements[10,18] but is in good agreement with the original study by Lozier and Niederberger[17] (see Table I). The origin of the literature disagreement may be associated with complex branching in the photocycle involving L (see Figure 1) and the fact that those measurements of χ_K^{500} lower than our number were both obtained on the basis of photocycle population studies involving intermediates that occur following L. An important point raised by Lozier and Niederberger[17] is that values of χ_K^{500} much lower than ~0.5 will produce anomalies in the calculated spectrum of K associated with the presence of unrealistically complex vibronic structure in the 23 000–27 000-cm^{-1} region of the 77 K spectrum (see Figure 4). Our spectrum of K at 77 K has a distinctly different high-energy vibronic development than that characteristic of the bR spectrum. Spectra of the K intermediate generated by assuming values of χ_K^{500} less than 0.42 display the same three vibronic maxima (~23 400, ~25 100, and 26 800 cm^{-1}) that are observed in the bR spectrum (although the intensity of these bands is much lower than that observed in the bR spectrum). We suggest that the probability that both bR and K have higher energy spectral bands at identical locations, while simultaneously displaying absorption maxima in the lower energy region that are shifted by > 1000 cm^{-1}, is unlikely in the extreme. Furthermore, the assumption of $\chi_K^{500} < 0.42$ corresponds to an upper limit of 0.35 for the quantum yield ratio (Φ_1/Φ_2) (Table II), a ratio which is smaller than that observed by the majority of previous investigations (Table I).

We determined, by using log-normal curve fitting techniques,[29] that the oscillator strength, f_{bR}, of the 77 K λ_{max} absorption band of bR shown in Figure 4 is 0.87. [We use the term "oscillator strength of the λ_{max} absorption band" to indicate that we are integrating under the entire absorption band, and thus the oscillator strength is likely the sum of contributions due to both the $^1B_u{}^{*+}$ and $^1A_g{}^{*-}$ excited states. The log-normal fitting technique ignores contributions from higher energy bands (see discussion in ref 29).] An analogous fit to the K spectrum (Figure 4) yields $d_K = 0.95$ (see Table II). Although the generation of an increased oscillator strength accompanying an all-trans to 13-cis photoisomerization may violate intuition, this observation is in keeping with previous experimental and theoretical studies which indicate that the separation of a protonated Schiff base chromophore from its primary counterion generates not only a red shift but also an increase in the oscillator strength of the λ_{max} absorption band.[29-31] The observation that $f_K > f_{bR}$ follows from an analysis of the 500-nm photostationary-state difference spectrum $\epsilon_K^{500} - \epsilon_{bR}^{500}$) shown in Figure 3. Note that generation of a photostationary state produces a difference spectrum which displays two distinct spectral regions. The lower energy region (13 000–22 600 cm^{-1}) displays a net oscillator strength increase of 0.037, whereas the higher energy region (22 600–28 200 cm^{-1}) displays a net oscillator strength decrease of −0.041. Accordingly, f_K must be larger than f_{bR} for the λ_{max} band, an observation independent of assignment of χ_K^{500}.

It is interesting to compare the results of the recent theoretical calculations of oscillator strength by Grossjean and Tavan[31] with our experimental measurements. These authors used PPP–MRD–CI molecular orbital procedures to calculate f values for all-trans, 13-cis, and 13-cis,14-s-cis retinyl protonated Schiff bases (RPSB). If we assume that the λ_{max} oscillator strengths are associated solely with the lowest lying $^1B_u{}^{*+} \leftarrow S_0$ transition and further assume that their calculation on the all-trans RPSB (3-Å counterion) simulates bR and their calculation on the 13-cis RPSB (no counterion) simulates K, the PPP–MRD–CI calculations predict a modest increase in oscillator strength from $f_{\text{all-trans}} = 1.12$ to $f_{\text{13-cis}} = 1.13$.[31] Although both values overestimate the oscillator strength, these calculations do predict an increase in going from bR to K. In contrast, if we make the identical assumptions for the bR simulation but use their calculation on the 13-cis,14-s-cis RPSB (no counterion) to simulate K, the PPP–MRD–CI calculations predict a decrease in oscillator strength ($f_{\text{13-cis,14-s-cis}} = 0.78$).[31] The latter simulation is relevant to the proposal of Tavan and Schulten[5a] that the primary event involves an all-trans to 13-cis,14-s-cis photoisomerization.[5] Although the failure of the theoretical results to simulate the correct trend in oscillator strength under this two-bond isomerization process does not preclude the viability of this mechanism, our experimental oscillator strength measurements suggest that the one-bond process

(29) Birge, R. R.; Einterz, C. M.; Knapp, H. M.; Murray, L. P. *Biophys. J.* **1988**, *53*, 367–385.
(30) Birge, R. R.; Pierce, B. M. In *Proceeding of the International Conference on Photochemistry and Photobiology*; Zewail, A. H., Ed.; Harwood Academic: New York, 1983; pp 841–855.
(31) Grossjean, M. F.; Tavan, P. *J. Chem. Phys.*, in press.

(all-trans → 13-cis) leads to a photoproduct that has a more realistic oscillator strength relative to that of the starting material at 77 K.

Energy Storage in the Primary Event. Values for the enthalpy stored in the K photoproduct, ΔH_{12}, as a function of Φ_1 are presented in the fourth column of Table III. The results of this study indicate that $\Phi_1/\Phi_2 = 0.445 \pm 0.031$, and thus $\Phi_1 \leq 0.48$ at 77 K. Accordingly, ΔH_{12} must be greater than 10 kcal mol^{-1} at 77 K. A more refined value for ΔH_{12}, however, can be assigned by adopting the forward and the reverse quantum yields measured by Hurley and Ebrey ($\Phi_1 = 0.33 \pm 0.05$, $\Phi_2 = 0.67 \pm 0.04$; ref 10). These latter assignments, when used in conjunction with our measured values of $\Phi_1/\Phi_2 = 0.445 \pm 0.031$, yield $\Delta H_{12} = 15.9 \pm 3.2$ kcal mol^{-1} on the basis of least-squares regression of eq 9–11. Our value for ΔH_{12} is very close to our previous measurement.[9] (The difference is due primarily to our use of different values for the molecular response function for experiments 2 and 3. It should be noted that the photocalorimetry data in ref 9 were analyzed on the basis of the Hurley and Ebrey quantum yield measurements.) Thus, the conclusions presented in ref 9 remain valid provided we can justify our adoption of the Hurley and Ebrey quantum yields. We believe that the Hurley and Ebrey measurements are valid for the present assignment for two reasons: (1) these investigators performed their measurements under experimental conditions identical with those adopted here, and (2) our measured quantum yield ratio is in excellent agreement with their assignment ($\Phi_1/\Phi_2 \sim 0.5$).

In order to evaluate the issue of energy storage in more detail, it is useful to provide a simple equation, based on our photocalorimetry measurements, that provides a method of calculating ΔH_{12} approximately based on alternative quantum yield assignments:

$$\Delta H_{12}\ (\text{kcal mol}^{-1}) \simeq \frac{1}{3}\left\{\frac{4.71}{\Phi_1} + \frac{12.0}{\Phi_2} + \frac{1}{0.10\Phi_2 + 0.0079\Phi_1}\right\} \quad (15)$$

Although application of this equation is not as rigorous as carrying out a weighted least-squares regression on eq 9–11, this equation predicts values of ΔH_{12} that agree within experimental error with those determined by the more accurate regression approach (Table IV). However, it is important to emphasize that the application of this equation carries with it the implicit assumption that the S_1* decay mechanisms are identical with those observed under the experimental conditions used to measure the molecular response function, Γ, determined here and implicit in the derivation of eq 15. Thus, if our model involving two distinct photocycles, bR_1 and bR_2, is correct, eq 15 cannot be used with confidence to assign energy storage for the bR_2 reaction cycle (Figure 5). With this restriction understood, however, it is illustrative to investigate the implications that those measurements generating values of Φ_1 greater than 0.6 would have on energy storage. The original measurement of the primary quantum yield of bR by Oesterhelt and Hess generated a value of $\Phi_1 = 0.79$. Because no measurement of Φ_2 was made, we must evaluate eq 15 as a function of Φ_2, which leads to the following results: $\Delta H_{12} = 9.1$ (1), 9.9 (0.9), 10.9 (0.8), 12.1 (0.7), 13.7 (0.6), 15.9 (0.5), 19.2 (0.4), and 24.5 (0.3) kcal mol^{-1} (Φ_2 in parentheses). A key observation is that these enthalpies are all larger than the value of ΔH_{12} predicted in Table III for a forward quantum yield of $\Phi_1 = 0.79$. This result is associated with the fact that the global least-squares regression analysis that was used to generate the values listed in Table III was not constrained to limit Φ_2 to values less than or equal to 1. Accordingly, the reader is cautioned not to assume that a forward quantum yield of $\Phi_1 = 0.79$ implies the small energy storage implied in Table III ($\Delta H_{12} \simeq 6.3$ kcal mol^{-1}).

It is interesting to compare the value we have determined at 77 K for glycerol/water solvent conditions with the values for ΔH_{12} obtained on the basis of other literature assignments of Φ_1 and Φ_2. Four separate investigations[10,12,13,19] report values for both Φ_1 and Φ_2, and the results along with calculated values of ΔH_{12} (eq 15) are presented in Table IV. Although the range in ΔH_{12} values on the basis of these results is fairly large ($13.9 \leq \Delta H_{12} \leq 19.3$ kcal mol^{-1}), the average of the four measurements is in excellent agreement with the value determined on the basis of Hurley and Ebrey's quantum yield measurements at 77 K.

Table IV. Energy Storage in the Primary Photoproduct, K, Calculated As a Function of Quantum Yield Assignments

source of quantum yield data[a]	Φ_1[b]	Φ_2[c]	ΔH_{12} (kcal mol^{-1})
Hurley and Ebrey (1978)[10]	0.33 ± 0.05	0.67 ± 0.04	**15.9 ± 3.2**[d]
Hurley and Ebrey (1978)[10]	0.33 ± 0.05	0.67 ± 0.04	15.7 ± 1.4[e]
Becher and Ebrey (1977)[13]	0.30 ± 0.03	0.77 ± 0.12	14.9 ± 2.0[e]
Goldschmidt et al. (1976)[12]	0.25 ± 0.05	0.63 ± 0.20	19.3 ± 5.3[e]
Dioumaev et al. (1988)[19]	0.31 ± 0.10	0.93 ± 0.14	13.9 ± 2.8[e]
Ref 10, 12, 13, and 19	0.30 ± 0.07[f]	0.75 ± 0.27[f]	16.0 ± 4.7[f]

[a] The data from ref 10 were obtained for 77 K solutions. The data from ref 12, 13, and 19 were obtained for ambient-temperature solutions. [b] Quantum yield for the formation of the primary photoproduct, K, from bR. [c] Quantum yield for the formation of bR from the primary photoproduct, K. [d] Calculated from a weighted least-squares regression (see text). This value is the preferred assignment of the energy storage. [e] Calculated with eq 15. The error range is determined on the basis of the assigned errors in Φ_1 and Φ_2 and does not include error associated with the photocalorimetry data used to generate eq 15. [f] These values were calculated by taking the average of the data listed in the preceding four rows of the same column. Error ranges are assigned conservatively as twice the standard deviation of the mean.

As noted in ref 9, our energy storage measurement is consistent with the detailed microphone calorimetry study of Ort and Parson.[32] These investigators measured an enthalpy storage of 15–20 kcal mol^{-1} ~100 μs after excitation. We conclude on the basis of arguments presented in ref 9 that this value is associated primarily with energy storage in the L intermediate. If we assume that K → L transition is entropy driven and/or involves a modest enthalpy change, our energy storage value and that measured by Ort and Parson should be very similar.

Energy Storage and Proton Pumping. Steady-state illumination of intact cells induces the light-adapted form of bacteriorhodopsin to eject one or more protons from the cytoplasm, generating an electrochemical gradient across the cell membrane.[2] This gradient can be partitioned into two components,[33-35]

$$\Delta p = \Delta\psi - 2.3RT\Delta\text{pH}/F \quad (16)$$

$$= \Delta\psi - 59\Delta\text{pH (mV at 25 °C)} \quad (17)$$

where Δp is the protonmotive force (or electrochemical gradient), $\Delta\psi$ is the electrical potential difference across the membrane, and ΔpH is the pH gradient across the membrane. Equation 17 is obtained by evaluating RT/F (R = gas constant, F = Faraday constant) at T = 298 K. The pH gradient during illumination is dependent upon extracellular pH as well as other factors and is thus subject to uncertainty. Estimates of ΔpH generally range from 0.7 to 1.5 units (inside alkaline).[35] Estimates of $\Delta\psi$ during illumination generally span the range from −120 to −220 mV.[35] Accordingly, the electrochemical gradient across the cell may reach ~300 mV, but for the purposes of this discussion we will assume a gradient of 250 mV (=$-\Delta p$).

The free energy required to pump a single proton across a gradient of 250 mV is ~6 kcal mol^{-1} (1 kcal mol^{-1} = 43.4 mV/molecule). For the purposes of this discussion, we will neglect entropy and assume the equivalence of enthalpy and free energy in estimating the relationship between energy storage and proton pumping capability. Under this approximation, the energy stored in the primary event (~16 kcal mol^{-1}) is sufficient to pump two, but not three, protons per photocycle under typical ambient

(32) Ort, D. R.; Parson, W. W. *Biophys. J.* **1979**, *25*, 35–364.
(33) Ferguson, S. J.; Sorgato, M. C. *Annu. Rev. Biochem.* **1982**, *51*, 185–199.
(34) Birge, R. R.; Lawrence, A. F.; Cooper, T. M.; Martin, C. T.; Blair, D. F.; Chan, S. I. In *Nonlinear Electrodynamics in Biological Systems*; Adey, W. R., Lawrence, A. F., Eds.; Plenum: New York, 1984; pp 107–120.
(35) Lanyi, J. K. *Microbiol. Rev.* **1978**, *42*, 682–712.

conditions. This maximum stoichiometry is consistent with many of the measurements of proton pumping stoichiometry, which indicate that two protons are pumped per photocycle.[6] However, as noted above, environments that select photocycles with primary quantum yields of $\Phi_1 \geq 0.6$ will likely result in a concomitant reduction in energy storage to $\sim$10 kcal mol^{-1} (e.g., Figure 5). The latter energy storage value is consistent with a proton pumping stoichiometry no larger than 1.

Biological Relevance of Two Photocycles. It is interesting to speculate on the potential biological relevance of our proposal that two photocycles may exist with different quantum yields and energy storage capacities. Following from our previous discussion, we will assign these two photocycles to have the following properties:

bR_1

$\Phi_1 \sim 0.3$ $\Delta H_{12} \sim 16$ kcal mol^{-1} [H]/photocycle = ~ 2 ($|\Delta p| \leq 250$ mV) and ~ 1 ($|\Delta p| > 250$ mV)

bR_2

$\Phi_1 \sim 0.6$ $\Delta H_{12} \sim 10$ kcal mol^{-1} [H]/photocycle = ~ 1 ($|\Delta p| \leq 250$ mV) and ~ 0 ($|\Delta p| > 250$ mV)

Following the model presented in Figure 6, we assign bR_2 as the lower free energy form of the protein that is nominally active under in vivo conditions. Natural selection may have designed bacteriorhodopsin to interconvert from bR_2 to bR_1 under conditions of high electrochemical gradient ($|\Delta p| > 250$ mV) where bR_2 is no longer capable of pumping a proton because the free energy stored is insufficient to override the membrane gradient. Because bR_1 stores more energy in the primary event, it is a more efficient proton pump under conditions of high membrane electrochemical gradient. Analysis of the data of Table I also suggests the possibility that bR_1 is photochemically selected via reverse photoreactions from K or M. Thus, under high light intensities, which will result in the generation of high electrochemical gradients, the protein is converted into the most efficient form. While the speculative nature of this discussion should be emphasized, we should not overlook the fact that the unusual photochemical properties of bacteriorhodopsin may have biological relevance.

Comments and Conclusions

(1) The ratio of the forward to reverse quantum yields (Φ_1/Φ_2) of light-adapted bacteriorhodopsin (bR) equals 0.45 ± 0.03 at 77 K. Thus, Φ_1 must be less than 0.48 under photostationary-state conditions at 77 K.

(2) The mole fraction of K (χ_K^{500}) in the 77 K, 500-nm photostationary state equals 0.46 ± 0.04. The absorption spectrum of K at 77 K has a maximum absorbance at 620 nm and a molar absorptivity at λ_{max} of $\sim$63 900 M^{-1} cm^{-1}. The oscillator strength associated with excitation into the λ_{max} band, f_K, is 0.95. The comparable values for bR at 77 K are λ_{max} = 577 nm, ϵ_{max} = $\sim$66 100 M^{-1} cm^{-1}, and f_{bR} = 0.87.

(3) The observation that $f_K > f_{bR}$ at 77 K is consistent with the displacement of the C_{15}=NH portion of the retinyl chromophore away from a negatively charged counterion as a consequence of the all-trans to 13-cis photoisomerization. It is difficult to reconcile the observation that $f_K > f_{bR}$ with the proposal that the primary event involves an all-trans to 13-cis,14-s-cis photoisomerization, because the latter geometry is predicted to have a significantly lower λ_{max} band oscillator strength relative to the all-trans precursor, regardless of counterion location.

(4) The primary photoproduct, K, has an enthalpy, ΔH_{12}, 15.9 ± 3.2 kcal mol^{-1} larger than that of bR at 77 K. This enthalpy assignment is not necessarily valid for those environments that yield primary quantum yields greater than or equal to 0.6.

(5) Experimental and theoretical evidence is presented which suggests the possibility that two distinct forms of light-adapted bacteriorhodopsin exist. These two forms have characteristic photocycles with significantly different primary quantum yields. INDO–PSDCI molecular orbital procedures and semiempirical molecular dynamics simulations predict that one ground-state geometry of bR yields $\Phi_1 \sim 0.27$ and a second ground-state geometry, with a slightly displaced counterion, yields $\Phi_1 \sim 0.74$. This theoretical model may explain the observation that literature measurements of Φ_1 tend to fall into one of two categories—those that observe $\Phi_1 \sim 0.33$ or below and those that observe $\Phi_1 \sim 0.6$ or above. The observation that all photostationary-state measurements of the primary quantum yield give values near 0.3 and all direct measurements of the quantum yield result in values near 0.6 suggests that photochemical back-reactions may select the bacteriorhodopsin conformation with the lower quantum yield.

Acknowledgment. This work was supported in part by grants from the National Institutes of Health (GM-34548), the National Science Foundation (CHE-8516155), and NAVAIR (MDA 903-86-M-1809).

Appendix

The principal goal of this appendix is to analyze the nature of the energy dependence of the molecular response function and provide a justification for using second-order polynomial regression in extrapolating the value of Γ_λ to zero pulse energy. Our discussion is prompted by the comment of a referee who noted that the use of polynomial regression appeared inconsistent with our prediction that at infinite pulse energy $\Gamma_\lambda = 1$. This comment was based in part on the observation that the polynomial curves shown in Figure 2 appear to extrapolate to $\Gamma_\lambda = -\infty$ for infinite pulse energy, a clearly inaccurate extrapolation. We will demonstrate, however, that, for pulse energies for which the number of solute molecules is at least 1 order of magnitude larger than the number of photons in the laser pulse, second-order polynomial regression is appropriate. At higher pulse energies, however, the molecular response function approaches unity as pulse energy increases in a near exponential fashion. We will also prove that the molecular response function equals unity for a photostationary-state mixture (no net photochemistry upon absorption of the pulsed laser excitation).

Energy Dependence of the Molecular Response Function. Our investigation of the energy dependence of Γ_λ in experiments 2 and 3 (see Experimental Section) is carried out by using numerical simulation. (As noted previously, experiment 1 did not reveal a pulse energy dependence within experimental error in the region 1–5 mJ/pulse.) Our simulations follow the numerical procedures presented in ref 36, and accordingly, our presentation will be limited to an analysis of those aspects of the simulation that are unique to this problem. The $\sim$3-mL volume of the photocalorimeter cell is divided into 1001 volume elements, and the solutes (bR and K) are assumed to be homogeneously distributed (prior to laser excitation) with the following initial concentrations for the 500-nm photostationary state: [bR] = 5.4×10^{-5} M; [K] = 4.6×10^{-5} M. The number of photons entering the solution for each laser pulse N_λ is given by

$$N_\lambda = \kappa E(\text{mJ})\lambda(\text{nm}) \times 5.034 \times 10^{12} \quad (18)$$

where κ is the fraction of the laser pulse that is not reflected off the surface of the calorimeter reaction solution, E(mJ) is the pulse energy in milliJoules, and λ(nm) is the wavelength of the laser irradiation in nanometers. The total number of molecules of species ξ promoted into the excited state within each reaction volume $N_{\Delta V}^*(\xi)$ is given by

$$N_{\Delta V}^*(\xi) = \min \{N_\lambda(1 - \exp[-3.82 \times 10^{-21}\epsilon_\lambda(\xi)C_{\Delta V}(\xi)\Delta l]), N_{\Delta V}(\xi)\} \quad (19)$$

where $\epsilon_\lambda(\xi)$ is the molar absorptivity of species ξ at the excitation wavelength, $C_{\Delta V}(\xi)$ is the concentration of species ξ in the volume element, Δl is the length in the direction of light propagation through the volume element, and $N_{\Delta V}(\xi)$ is the number of species ξ in the volume element prior to laser excitation. The min function limits the number of excited-state species to a value less than or

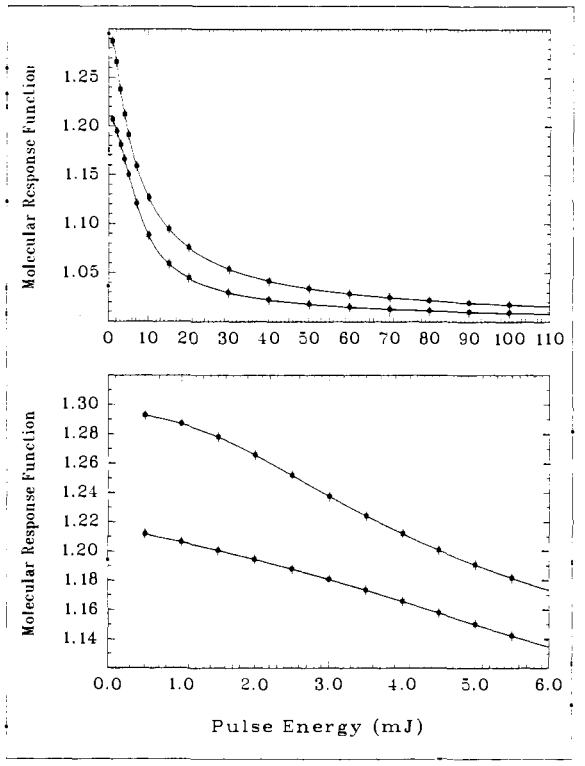

Figure 7. Results of numerical simulations of the energy dependence of Γ_λ for the conditions encountered in experiments 2 and 3 for the pulse energy range 0.5–110 mJ (top) and 0.5–6 mJ (bottom). The top graph displays the exponential dependence that is expected intuitively and extrapolates to $\Gamma_\lambda = 1$ for $E_{mJ} = \infty$. The lower energy region analyzed in the lower graph, however, exhibits a quadratic dependence which can be fit with accuracy by the function $\Gamma_\lambda = A + B(E_{mJ}) + C(E_{mJ})^2$ (see Appendix). For both graphs, the simulations for experiment 2 are shown in the top curves, and the simulations for experiment 3 are shown in the bottom curves.

equal to the number of ground-state species within the volume element. (Our numerical procedures do allow, however, for multiple excitation of a given molecule during the time interval of the laser pulse.) Photochemistry within the volume element generates a new distribution of species on the basis of the number of excited states generated and the quantum yields of conversion:

$$\Delta N(\mathrm{bR})_{\Delta V} = \Phi_2 N_{\Delta V}^*(\mathrm{K}) - \Phi_1 N_{\Delta V}^*(\mathrm{bR}) \qquad (20a)$$

$$\Delta N(\mathrm{K})_{\Delta V} = \Phi_1 N_{\Delta V}^*(\mathrm{bR}) - \Phi_2 N_{\Delta V}^*(\mathrm{K}) \qquad (20b)$$

Conservation of mass requires that $\Delta N(\mathrm{bR})_{\Delta V}$ equals $-\Delta N(\mathrm{K})_{\Delta V}$. The photochemical reactions that occur in the photocalorimeter cell will generate, under non-photostationary-state conditions, a redistribution of the species that will either store or release energy. The molecular response function is the normalized measure of this process and is larger than unity when energy is released and smaller than unity when energy is stored. For the numerical simulation described above, this function is calculated as follows:

$$\Gamma_\lambda = 1 + \frac{1}{2}\left(\frac{\Delta N(\mathrm{bR})_{TOT}}{N^*_{TOT}}\frac{\Delta H_{12}}{\Delta H_{photon}} - \frac{\Delta N(\mathrm{K})_{TOT}}{N^*_{TOT}}\frac{\Delta H_{12}}{\Delta H_{photon}}\right) \qquad (21a)$$

$$\Gamma_\lambda = 1 + \frac{\Delta N(\mathrm{bR})_{TOT}}{N^*_{TOT}}\frac{\Delta H_{12}}{\Delta H_{photon}} \qquad (21b)$$

where $\Delta N(\mathrm{bR})_{TOT}$ is the change in the number of bR species in the total reaction volume and N^*_{TOT} is the total number of photons absorbed by all species present. Conservation of mass yields the symmetry that permits reduction of eq 21a to eq 21b. Our simulation neglects absorption of light by impurities in the solution as well as the cell walls and impurities. Because of this neglect, our simulation will overestimate the deviation of Γ_λ from unity at high pulse energies. This observation follows from the fact that the absorption of light by any nonphotochemical component will minimize deviation of the observed response function from unity. Because we are interested primarily in the low pulse energy behavior, we do not view this simplification in our numerical procedures to be relevant to the present analysis.

Simulations were carried out for the experimental conditions associated with experiments 2 and 3, and the results are presented in Figure 7. It is clear that the pulse energy dependence of Γ_λ is very different at low pulse energy (0–6 mJ) versus high pulse energy (6–100 mJ). The latter region displays the exponential dependence that is expected intuitively and extrapolates to $\Gamma_\lambda = 1$ for $E_{mJ} = \infty$. The lower energy region, however, has a quadratic dependence which can be fit with excellent accuracy by the function $\Gamma_\lambda = A + B(E_{mJ}) + C(E_{mJ})^2$, which is the function that we used to assign the zero pulse energy value for Γ_λ ($=A$). This quadratic behavior can be traced to the fact that at moderate to low pulse energies (for the present case, $E_{mJ} < 10$ mJ/pulse) the number of absorbing species within the irradiated volume far exceeds the number of photons entering the photocalorimeter cell. Thus, the ratio $\{\Delta N(\mathrm{bR})_{TOT}\}/N^*_{TOT}$ remains fairly constant in this pulse energy region. It is only at pulse energies in which the number of photons in the laser pulse approaches or exceeds the number of absorbing species that the exponential dependence observed in Figure 7 (top) dominates.

Proof That $\Gamma_\lambda = 1$ for the λth Photostationary State. It is also useful to demonstrate why the molecular response function, Γ_λ, equals unity for the photostationary state generated by excitation at wavelength λ, because this is a key element of our use of the photostationary state as an internal standard (see discussion in ref 9). First, it should be noted that the situation we are evaluating involves the photostationary state associated with the pulsed laser excitation wavelength, and not the photostationary state prepared via illumination at a different wavelength prior to carrying out the photocalorimetric measurement. The key element that determines a photostationary state is that no pet photochemical reactions take place as a result of the absorption of light at the photostationary-state wavelength. Accordingly, $\Delta N(\mathrm{bR})_{TOT} = \Delta N(\mathrm{K})_{TOT} = 0$, and the right-hand side of eq 21 equals unity. It is more difficult to demonstrate that $\Gamma_\lambda = 1$ on the basis of the equation which we use to relate the molecular response function to the enthalpy difference, ΔH_{12}, for photostationary-state conditions:

$$\Gamma_\lambda = \alpha_{\lambda_{exc}}^{\lambda_{prep}}(1 - \Phi_1\mathcal{R}) + (1 - \alpha_{\lambda_{exc}}^{\lambda_{prep}})(1 + \Phi_2\mathcal{R}) \qquad (22)$$

where

$$\mathcal{R} = \Delta H_{12}/\Delta H_{photon} \qquad (23)$$

The key to the analysis of eq 22 is to recognize that the relative concentrations of bR and K obey the following relationship for a photostationary state:

$$\frac{\Phi_1}{\Phi_2} = \frac{\epsilon_K^{500}}{\epsilon_{bR}^{500}}\frac{[\mathrm{K}]}{[\mathrm{bR}]} \qquad (24)$$

Accordingly

$$\alpha_{\lambda_{exc}}^{\lambda_{prep}} = [\mathrm{bR}]\epsilon_{bR}^{\lambda_{exc}}/([\mathrm{bR}]\epsilon_{bR}^{\lambda_{exc}} + [\mathrm{K}]\epsilon_K^{\lambda_{exc}}) = (1 + \Phi_1/\Phi_2)^{-1} \qquad (25)$$

Substitution of eq 25 into eq 22 yields

$$\Gamma_\lambda = \frac{1 - \Phi_1\mathcal{R}}{1 + \Phi_1/\Phi_2} + \frac{1 + \Phi_1\mathcal{R}}{1 + \Phi_1/\Phi_2} + 1 + \Phi_2\mathcal{R} = \frac{1 + \Phi_1/\Phi_2}{1 + \Phi_1/\Phi_2} = 1 \qquad (26)$$

Note, in particular, that this result is independent of both ΔH_{12} and ΔH_{photon}, which is key to the use of the photostationary state as an internal standard.